Supplement of Geosci. Model Dev., 19, 4857–4883, 2026
https://doi.org/10.5194/gmd-19-4857-2026-supplement

Geoscientific Model Development
Open Access
EGU

Supplement of

AgPaDS v1.0: a GPU-accelerated interactive Lagrangian atmospheric transport model with 3-D in situ visualization for simulating windborne dispersal of crop pathogens

Marcel Meyer et al.

Correspondence to: Marcel Meyer (mmeyer2@uni-bonn.de)

Supplementary Information

Model description 3
Figure S1: AgPaDS architecture: inputs, core components & outputs 3
Table S1: Selected AgPaDS simulation parameters with examples for process- and data-based definitions and options for interactive configuration 4
Figure S2: Overview AgPaDS class structure – selected classes with key methods and members 5
Model testing 6
Table S2: Source locations and release date for AgPaDS and HYSPLIT test runs 6
Figure S3: Screenshot of the NVIDIA Nsight Systems tool illustrating the tracing of AgPaDS computations over one timestep of meteorological data. 7
Figure S4: Screenshot of the NVIDIA Nsight Systems tool illustrating the tracing of AgPaDS computations over one time-step of Lagrangian particle integration. 8
Table S3: Interactive and in situ visualization methods - key aspects of technical implementation and potential use-cases 9
Figure S5: Comparison of mean trajectories computed by AgPaDS and HYSPLIT from a source in Argentina at three different release altitudes 11
Figure S6: Comparison of stochastic Lagrangian particle modelling output computed by AgPaDS and HYSPLIT for a source in Argentina 12
Figure S7: Comparison of mean trajectories computed by AgPaDS and HYSPLIT from a source in Australia at three different release altitudes 13
Figure S8: Comparison of stochastic Lagrangian particle modelling output computed by AgPaDS and HYSPLIT for a source in Australia 14
Figure S9: Comparison of mean trajectories computed by AgPaDS and HYSPLIT from a source in China at three different release altitudes 15
Figure S10: Comparison of stochastic Lagrangian particle modelling output computed by AgPaDS and HYSPLIT for a source in China 16
Figure S11: Comparison of mean trajectories computed by AgPaDS and HYSPLIT from a source in Denmark at three different release altitudes 17
Figure S12: Comparison of stochastic Lagrangian particle modelling output computed by AgPaDS and HYSPLIT for a source in Denmark 18
Figure S13: Comparison of mean trajectories computed by AgPaDS and HYSPLIT from a source in Ethiopia at three different release altitudes 19
Figure S14: Comparison of stochastic Lagrangian particle modelling output computed by AgPaDS and HYSPLIT for a source in Ethiopia 20
Figure S15: Comparison of mean trajectories computed by AgPaDS and HYSPLIT from a source in India at three different release altitudes 21
Figure S16: Comparison of stochastic Lagrangian particle modelling output computed by AgPaDS and HYSPLIT for a source in India 22
Figure S17: Comparison of mean trajectories computed by AgPaDS and HYSPLIT from a source in Iran at three different release altitudes 23

Figure S18: Comparison of stochastic Lagrangian particle modelling output computed by AgPaDS and HYSPLIT for a source in Iran 24
Figure S19: Comparison of mean trajectories computed by AgPaDS and HYSPLIT from a source in Italy at three different release altitudes 25
Figure S20: Comparison of stochastic Lagrangian particle modelling output computed by AgPaDS and HYSPLIT for a source in Italy 26
Figure S21: Comparison of mean trajectories computed by AgPaDS and HYSPLIT from a source in Kazakhstan at three different release altitudes 27
Figure S22: Comparison of stochastic Lagrangian particle modelling output computed by AgPaDS and HYSPLIT for a source in Kazakhstan 28
Figure S23: Comparison of mean trajectories computed by AgPaDS and HYSPLIT from a source in Morocco at three different release altitudes 29
Figure S24: Comparison of stochastic Lagrangian particle modelling output computed by AgPaDS and HYSPLIT for a source in Morocco 30
Figure S25: Comparison of mean trajectories computed by AgPaDS and HYSPLIT from a source in Mexico at three different release altitudes 31
Figure S26: Comparison of stochastic Lagrangian particle modelling output computed by AgPaDS and HYSPLIT for a source in Mexico 32
Figure S27: Comparison of mean trajectories computed by AgPaDS and HYSPLIT from a source in Pakistan at three different release altitudes 33
Figure S28: Comparison of stochastic Lagrangian particle modelling output computed by AgPaDS and HYSPLIT for a source in Pakistan 34
Figure S29: Comparison of mean trajectories computed by AgPaDS and HYSPLIT from a source in Russia at three different release altitudes 35
Figure S30: Comparison of stochastic Lagrangian particle modelling output computed by AgPaDS and HYSPLIT for a source in Russia 36
Figure S31: Comparison of mean trajectories computed by AgPaDS and HYSPLIT from a source in South-Africa at three different release altitudes 37
Figure S32: Comparison of stochastic Lagrangian particle modelling output computed by AgPaDS and HYSPLIT for a source in South-Africa 38
Figure S33: Comparison of mean trajectories computed by AgPaDS and HYSPLIT from a source in USA at three different release altitudes. 39
Figure S34: Comparison of stochastic Lagrangian particle modelling output computed by AgPaDS and HYSPLIT for a source in USA 40
Figure S35: Comparison of time-backwards mean trajectories in HYSPLIT and AgPaDS. 41
Figure S36: Performance measurements of baseline implementations 41
Model discussion 42
Table S4: AgPaDS domains of use – discussion of applicability and feasibility 42

Model description

Figure S1: AgPaDS architecture: inputs, core components & outputs

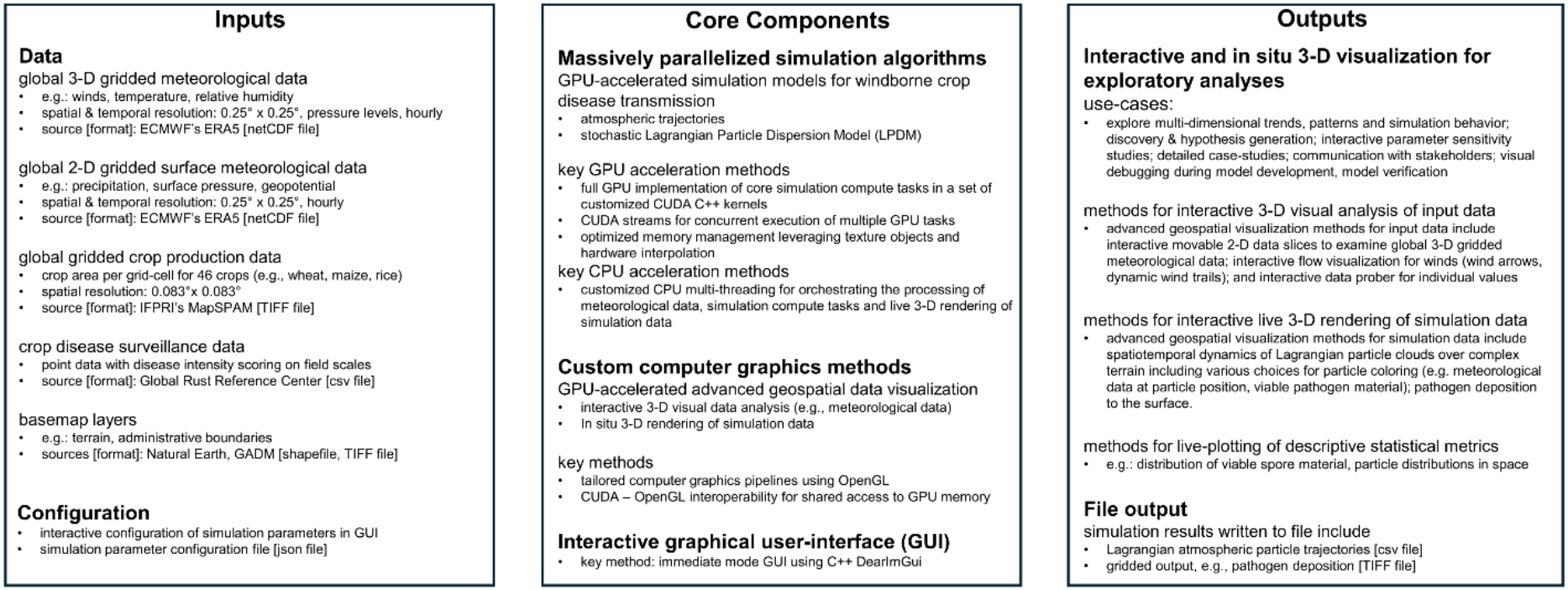

Table S1: Selected AgPaDS simulation parameters with examples for process- and data-based definitions and options for interactive configuration

Parameter Name	Notation	Example for process- or data-based constraints/definition	Option for interactive configuration in GUI
Source types: point source, rectangular source, gridded source			
source centre location	$S_{\lambda\phi z}$	disease outbreak data	yes
geographical extent	$\Delta\lambda, \Delta\phi, \Delta z$	disease outbreak data	yes
source timing	t_{source}	spore release timing from published field experiments	yes
total source material	M	estimate based on infected area, disease severity & intensity	yes
Atmospheric transport types of transport models: deterministic trajectories, stochastic Lagrangian particle dispersion			
number of trajectories / Lagrangian particles	N	typical values from atm. transport modelling for use-case	yes
activate mesoscale motion	δ_{meso}	consider dominant wind flow regimes for use-case	yes
activate turbulence	δ_{turb}	consider dominant wind flow regime for use-case	yes
activate sedimentation	δ_{sed}	pathogen characteristics (e.g., size, density)	yes
particle integration step	Δt	typical values from atm. modelling; resolution of input data	yes
Viability decay types of viability decay models: binary, time-dependent, critical UV dose, RH dependent UV dose			
maximum lifetime	t_{max}	lab experiments	yes
constant decay rate	d	lab experiments	yes
critical UV dose	κ	lab/controlled field experiments	yes
sensitivity to UV dose	K	lab/controlled field experiments	yes
Deposition types of deposition models: dry deposition, wet deposition			
dry deposition velocity	v_{dry}	lab experiments	yes
critical precipitation	p_{crit}	estimate from aerosols of similar siz	no

Figure S2: Overview AgPaDS class structure – selected classes with key methods and members

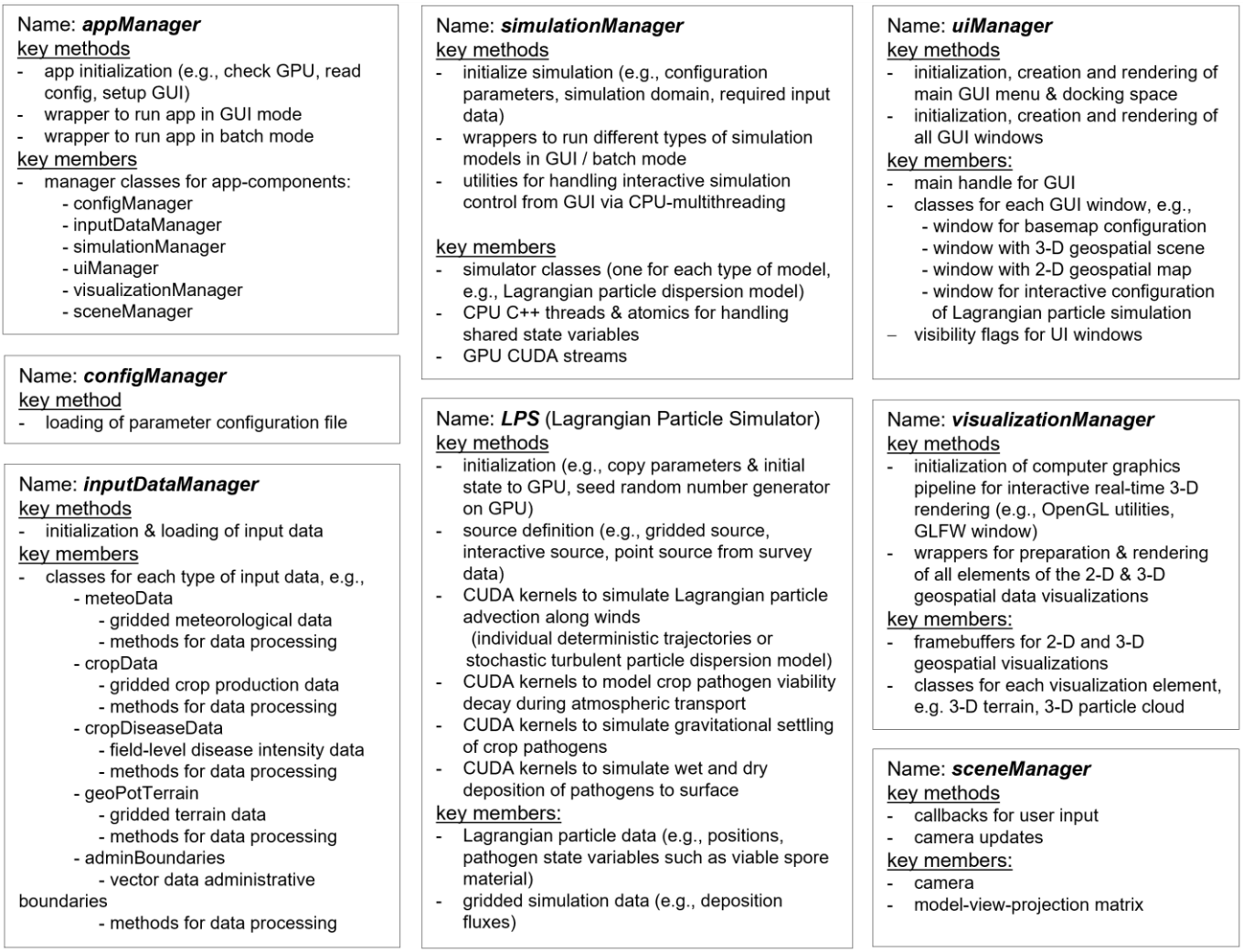

Model testing

Table S2: Source locations and release date for AgPaDS and HYSPLIT test runs

ID	**Source name**	**Coordinates** [latitude, longitude]	**Release time** [12:00 noon UTC]
1	Argentina	[-31.7, -61.7]	15/12/2024
2	Australia	[-30.7, 117.1]	15/11/2024
3	China	[34.2, 115.5]	15/06/2024
4	Denmark	[56.3, 9.9]	15/07/2024
5	Ethiopia	[7.2, 39.1]	15/12/2024
6	India plains	[27.1, 77.8]	15/03/2024
7	Iran	[35.7, 48.1]	15/06/2024
8	Italy south	[37.6, 13.8]	15/06/2024
9	Kazakhstan	[52.8, 66.0]	15/07/2024
10	Morocco	[32.4, -8.5]	15/05/2024
11	Mexico	[20.6, -101.6]	15/05/2024
12	Pakistan coast	[25.8, 68.5]	15/03/2024
13	Russia	[48.0, 41.6]	15/07/2024
14	Southern Africa	[-28.15, 26.3]	15/10/2024
15	USA	[37.2, -97.9]	15/05/2024

Figure S3: Screenshot of the NVIDIA Nsight Systems tool[1] illustrating the tracing of AgPaDS computations over one timestep of meteorological data.

(i) the area highlighted by the upper red rectangle shows the execution of tasks in different CUDA streams, such as the memory transfer operation to copy meteorological data from CPU to GPU in stream 13 and the repeated CUDA Kernel for each timestep of Lagrangian particle integration in stream 14, along with OpenGL processing for live rendering.

(ii) the area highlighted by the lower red rectangle shows NVTX ranges set to measure the start and end time of different computational tasks, confirming the concurrent execution of key CPU and GPU tasks: loading meteorological data from disk to GPU memory; transfer meteorological data from CPU to GPU; Lagrangian atmospheric transport calculations, such as particle integration, on GPU. See Figure S3 for zoom into one particle integration step.

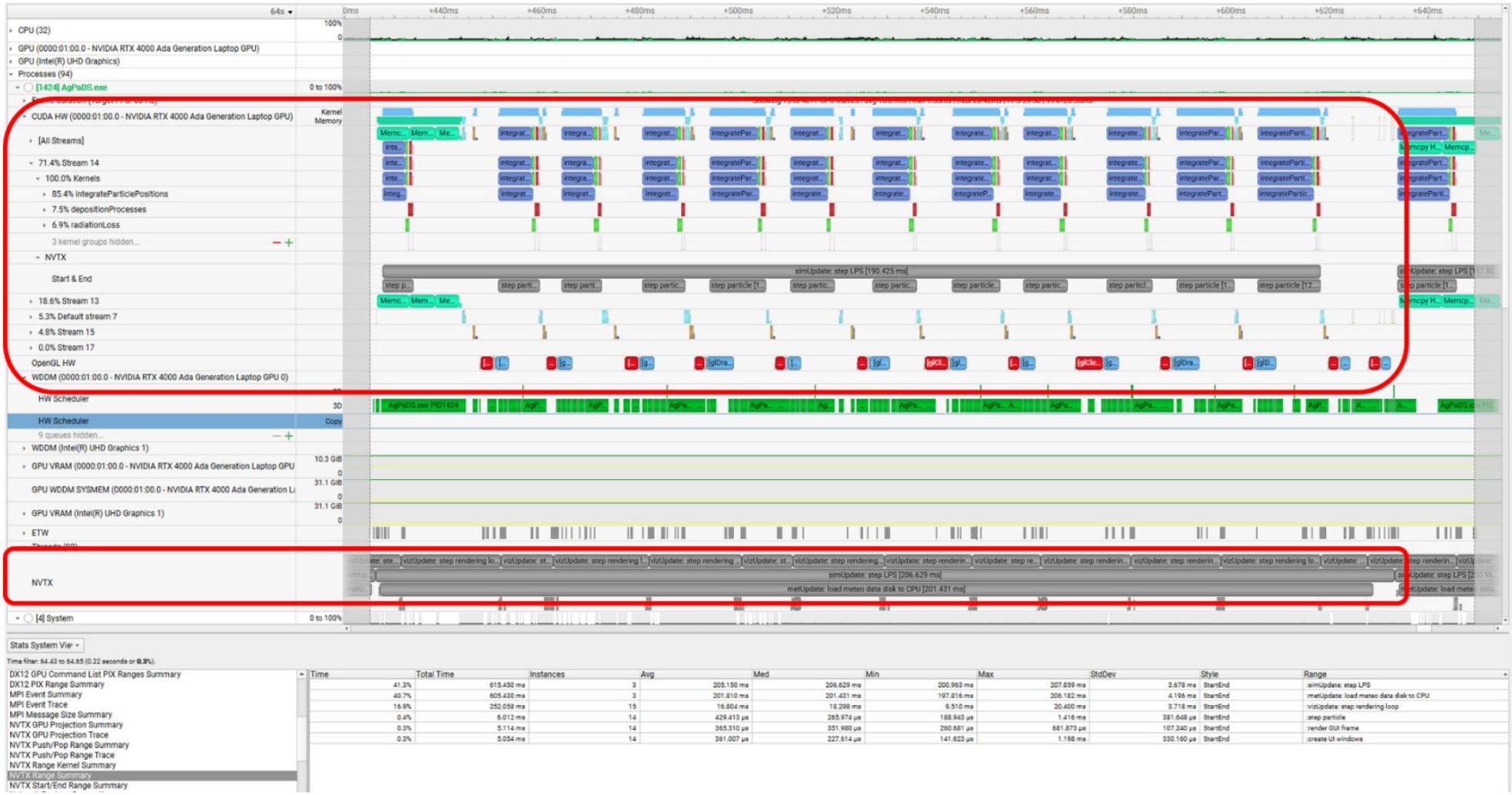

[1] see: https://docs.nvidia.com/nsight-systems/UserGuide/index.html *[last accessed: 01/06/2026]*

Figure S4: Screenshot of the NVIDIA Nsight Systems tool[1] illustrating the tracing of AgPaDS computations over one time-step of Lagrangian particle integration.

(i) the area highlighted by the upper red rectangle shows the concurrent execution of memory transfer and Lagrangian atmospheric transport calculations in CUDA kernels for particle integration, viability loss and pathogen deposition.

(ii) the area highlighted by the middle red rectangle shows OpenGL processes for in-situ visualization of Lagrangian transport simulations.

(iii) the lower red rectangle shows NVTX ranges set to measure different computational processes, including the update of the simulation state and the in-situ visualization.

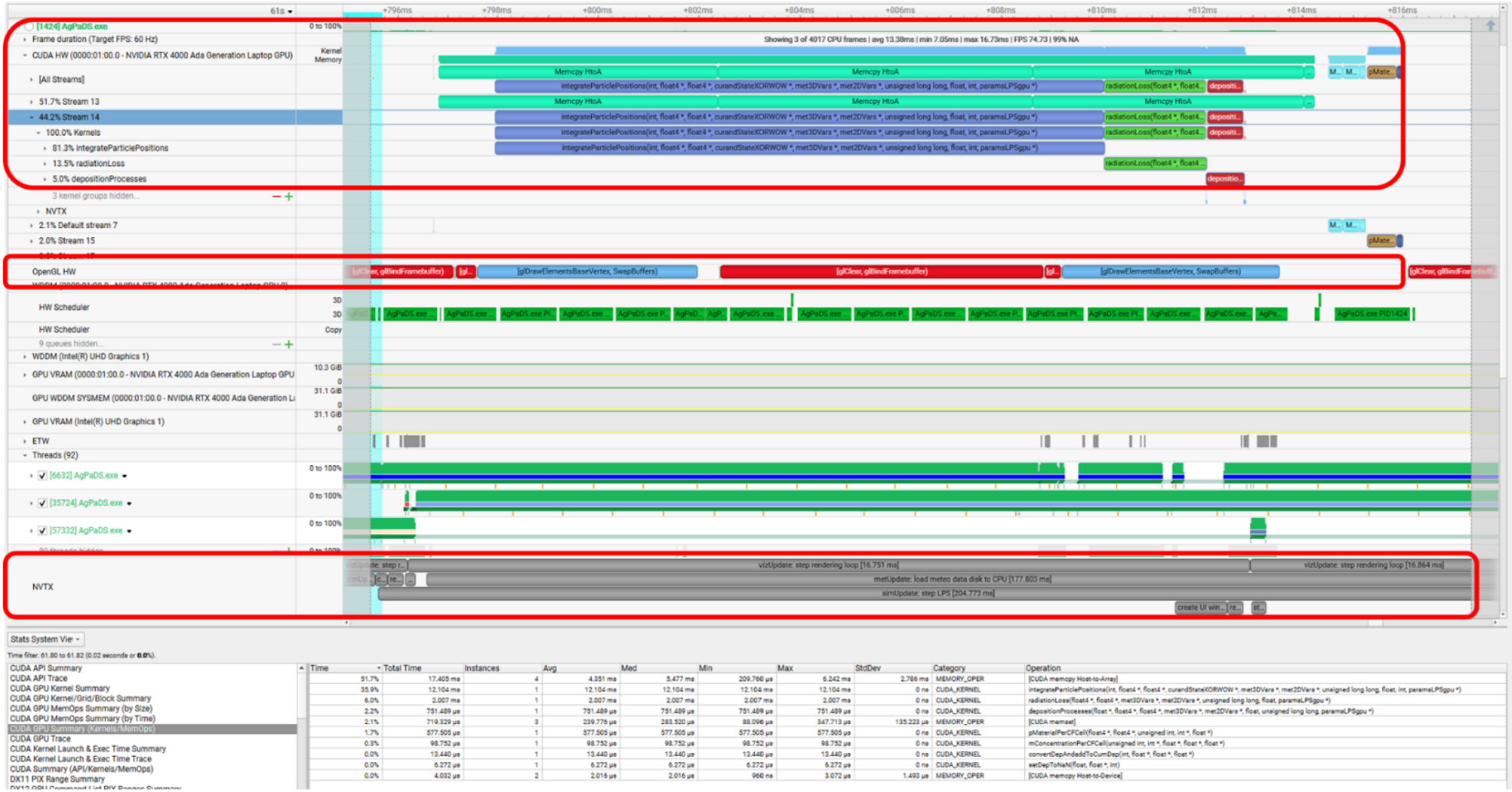

[1] see: https://docs.nvidia.com/nsight-systems/UserGuide/index.html *[last accessed: 01/06/2026]*

Table S3: Interactive and in situ visualization methods - key aspects of technical implementation and potential use-cases

	description	summary of technical implementation	use-cases	GUI screen recording

1	**selection of geospatial view mode**
	- 2-D map view
	- 3-D scene view:
	  - globe view [rotating sphere]
	  - box view [latitude, longitude, pressure]
	- support for concurrent visualization of one 2-D map and one 3-D scene in two different GUI windows
		- custom *OpenGL* shader code and GUI elements
		- *OpenGL* vertex shaders handle the transformation between spherical and cartesian coordinates for switching between the two 3-D views
		- visualizations are rendered to an offscreen OpenGL framebuffer that is integrated into the *DearImGUI* window as a texture image
			- inspect input and simulation data from different spatial perspectives
			- examples
			(i) examination of 3-D spatiotemporal dynamics of atmospheric transport,
			(ii) analyses of meteorological drivers affecting pathogen transmission (e.g., winds, humidity, temperature)
				Movie S2

2	**interactive camera system** - interactive geospatial visualization of 2-D and 3-D input and simulation data as viewed through a hypothetical camera that is steered by the user (e.g., setting camera position and angle) - 2-D map: zooming in/out & panning - 3-D scene: free fly & orbiting camera features	- *GLFW* and *ImGUI* callbacks for user-interaction via keyboard & mouse - *C++ GLM* for coordinate transformation matrices - custom *OpenGL* shader code and GUI elements	- navigation and visual examination of complex time-dependent 3-D geospatial data (live simulation data, input data) - enable exploratory analyses by generating multidimensional insights, facilitating detection of patterns, hypothesis formulation, visual debugging, model verification	Movie S3
3	**configuration of basemap layers** - coastlines - administrative boundaries (level 0 and 1) - land-sea mask - graticule and gridlines along pressure levels text labels	- custom *OpenGL* shader code and GUI elements - loading of vector data for basemap layers adapted from *Met.3D* - rendering of labels in 3-D scene based on *OpenGL* text rendering	- configure basemap layers to provide geographical context and spatial references for the main visualization	Movie S4
4	**terrain rendering** - 2-D terrain - 3-D terrain - lighting/shading features to improve spatial perception of complex terrain	- custom *OpenGL* shader code, *CUDA* kernels, and GUI elements - 2-D basemap visualization adapted from *Met.3D* - 3-D terrain visualization based on custom *CUDA* kernels and OpenGL shaders to create and render vertex data (e.g., triangle mesh, texture coordinates, surface normals)	- geographical orientation - detailed case analyses in areas with complex terrain - realism for communication visuals	Movie S5

5	**interactive visualization of raster data (e.g., crop mask, 2-D surface meteorology, deposition)**
	- selection of data file and variable for visual analysis as 2-D map or in 3-D scene
	- user-defined colormaps, transparency & legends
	- basic data processing (e.g., log-scale, thresholds)
	- support for time-stepping and time-streaming
		- custom *OpenGL* shader code, *CUDA* kernels, and GUI elements
		- *CUDA* kernels read data of interest from GPU memory, map it to RGBA color values and write these to a GPU texture object for *OpenGL* rendering
		- supports both in-situ visualization of live simulation data and visualization of pre-loaded gridded input data
			- interactive visual analyses 2-D gridded input data (e.g., crop mask) and simulation data (e.g., gridded pathogen deposition)
			- examples:
			  - exploratory examination of spatiotemporal patterns,
			  - detailed case analyses,
			  - visual debugging and model verification
				Movie S6

6	**interactive visualization of point data (e.g., crop disease surveillance data)** - selection of data file for visual analysis as 2-D map or in 3-D scene - support for time-scaping for analysis of disease dynamics	- custom *OpenGL* shader code and ImGUI methods for data loading and interactive configuration	- visualization of crop disease surveillance data, including temporal changes in spatial point patterns	Movie S7

7	**movable data slices for interactive visualization of 3-D global meteorological data**
	- 2-D planes that can be moved interactively to slice through gridded 3-D meteorological data volumes,
	  - lat-lon plane moving through pressure levels
	  - lat-pressure plane moving along longitudes
	  - lon-pressure plane moving along latitudes
	- support for time stepping and time-streaming of
		- custom *OpenGL* shader code, *CUDA* kernel, and GUI elements
		  - *CUDA* kernels conduct cached reading of meteorological data with hardware accelerated interpolation from data grid to sub-grid position of the slicing planes, convert data values to RGBA color codes and write these to a texture object for live rendering via OpenGL graphics pipeline
			- visual examination of complex 3D global meteorological data, e.g. to identify key drivers affecting pathogen biology	Movie S8

	meteorological input data			
8	**interactive data prober** - movable point probe to sample individual data values at specific positions in 3D data volume	- custom *OpenGL* shader code, *CUDA* kernel, and GUI elements - the *CUDA* kernel reads & interpolates meteorological data from grid to sub-grid position of interactive probe particle	- inspect individual data values, e.g. for detailed case analyses or visual debugging and model verification	Movie S9
9	**flow visualization for wind data** - wind arrows - dynamic wind trails - rendered on horizontal data plane that can be - moved vertically along pressure levels	- custom *OpenGL* shader code, *CUDA* kernel, and GUI elements - CUDA kernels compute the wind arrow geometry and dynamic trail positions based on wind magnitude and direction	- explore wind data as key driver for windborne crop disease transmission and key input for Lagrangian particle model - movable plane enables e.g. the examination of changes in wind direction and magnitude with varying altitudes	Movie S10
10	**interactive Lagrangian particle source definition (e.g., gridded source clipped to crop growing areas)** - the coordinates, geographical extent and type of the source term for Lagrangian particle transport simulations can be defined interactively - e.g., individual rectangular sources or gridded release from crop landscape	- custom *OpenGL* shader code, and GUI elements - source geometry input from user is mapped to OpenGL vertex data for rendering and passed to the Lagrangian particle simulator to initialize the source term.	- start Lagrangian particle simulations interactively relative to other elements in the 3-D scene (e.g., crop areas, terrain, meteorological data) to enable exploratory visual analyses of particle transport along winds - as the exact source location for pathogen release is often associated with large uncertainties in available empirical data, this allows screening large potential areas to identify areas and times of particularly high/low risks	Movie S11

11	**interactive Lagrangian particle simulation**
	- rendering Lagrangian point particles as small spheres with basic lighting/shading for improved spatial perception
	- interactive selection of particle coloring according to
	  o meteorological data at particle position
	  o particle age
	  o cumulative UV dose along particle trajectory
	  o viable pathogen material on particle
		- custom *OpenGL* shader code, *CUDA* kernels and GUI elements
		- *CUDA* kernel maps data of interest to RGBA color values for particle spheres
		- *OpenGL* and *CUDA* access the same GPU memory buffers (particle positions and state) for rendering and simulation purposes which facilitates real-time 3-D visualization at simulation runtime.
			- interactive visual analyses of complex atmospheric transport processes
			- examine meteorological drivers that affect pathogen biology during atmospheric transport (e.g., temperature, cumulative UV dose)
			- examine changes of biological state variables (e.g., viable spore material) during atmospheric transport
			- detailed case analyses, e.g. meteorological extreme event causing disease transmission
			- visual debugging and model verification
				Movie S12

12	**interactive particle viewing windows** - transparent 2-D planes that can be moved to slice through 3-D Lagrangian particle clouds at specific positions	- custom *OpenGL* shader code, and GUI elements - *OpenGL* vertex/fragment shaders used to set visibility of particles conditional on position relative to viewing window	- examine 3-D structure of Lagrangian particle clouds, meteorological drivers and biological state variables of Lagrangian particle clouds, e.g. for detailed case analyses of complex windborne transport patterns	Movie S13
13	**2-D charts summarizing simulation data statistics** - e.g., histograms showing the distribution of viable spore material on all Lagrangian particles at runtime	- *ImPlot* library in combination with *ImGUI* to integrate interactive 2D charts into the GUI - custom *CUDA* kernels using amongst others parallel reduction techniques for efficient massively parallelized computation of Lagrangian particle statistics at run-time	- in-situ analysis of simulation data at run-time (e.g., spatial distribution of Lagrangian particles, distribution of viable spore material carried by simulation particles)	Movie S14

Figure S5: Comparison of mean trajectories computed by AgPaDS and HYSPLIT from a source in Argentina at three different release altitudes

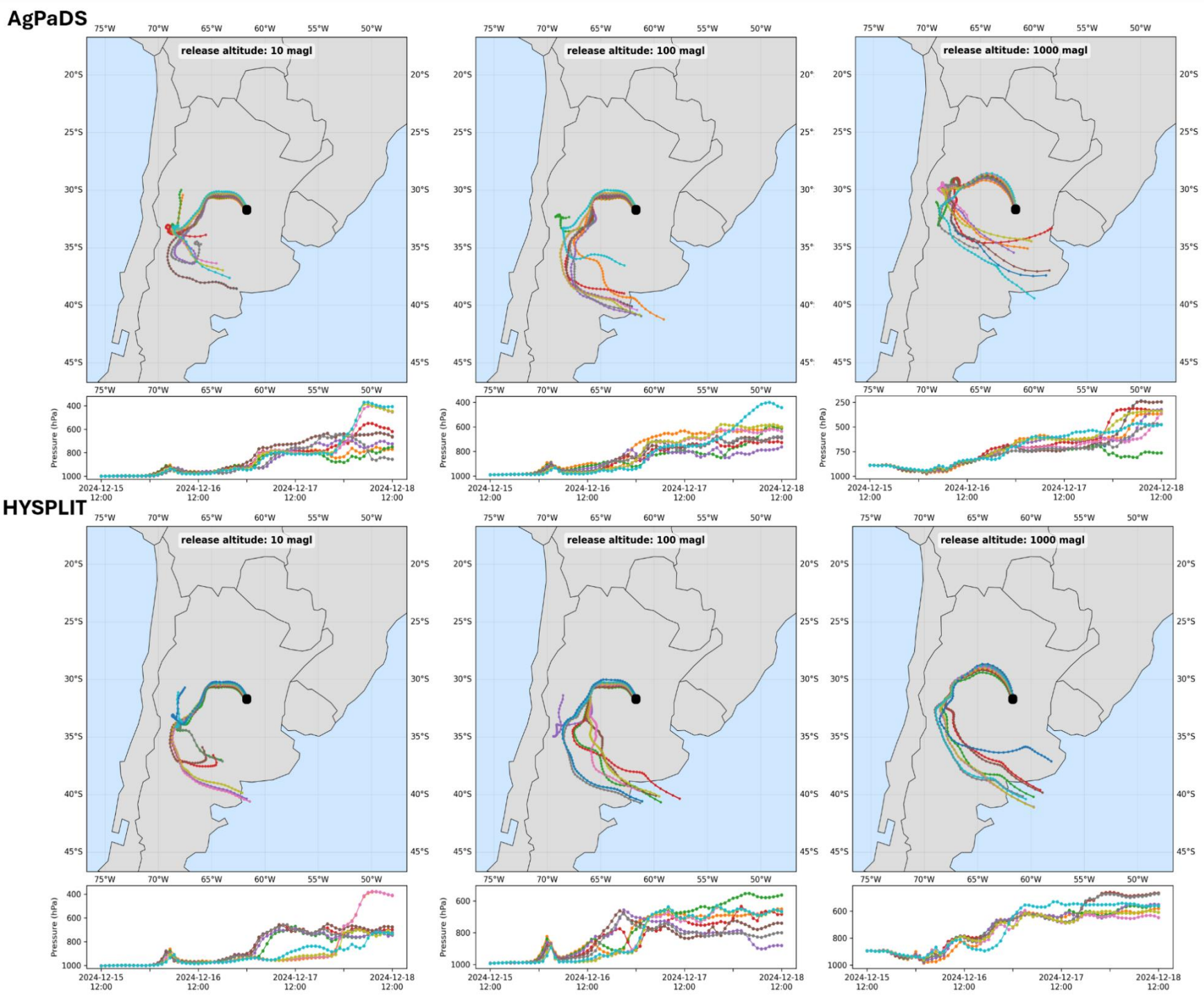

Figure S6: Comparison of stochastic Lagrangian particle modelling output computed by AgPaDS and HYSPLIT for a source in Argentina

(a) top row: cumulative deposition at t=48h after release; bottom row: instantaneous particle plume in air at t=48h after release.

(b) deposition plume overlap.

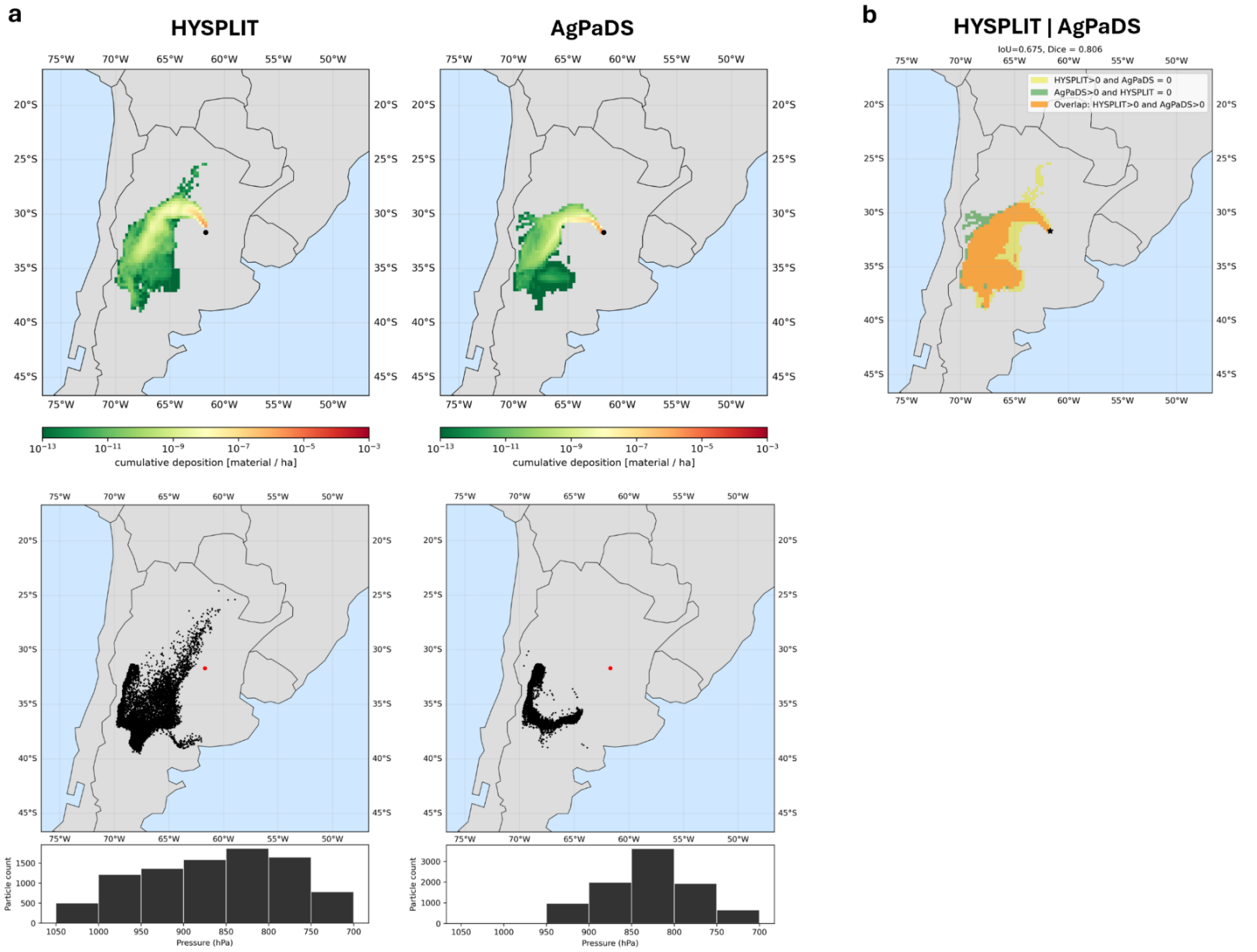

Figure S7: Comparison of mean trajectories computed by AgPaDS and HYSPLIT from a source in Australia at three different release altitudes

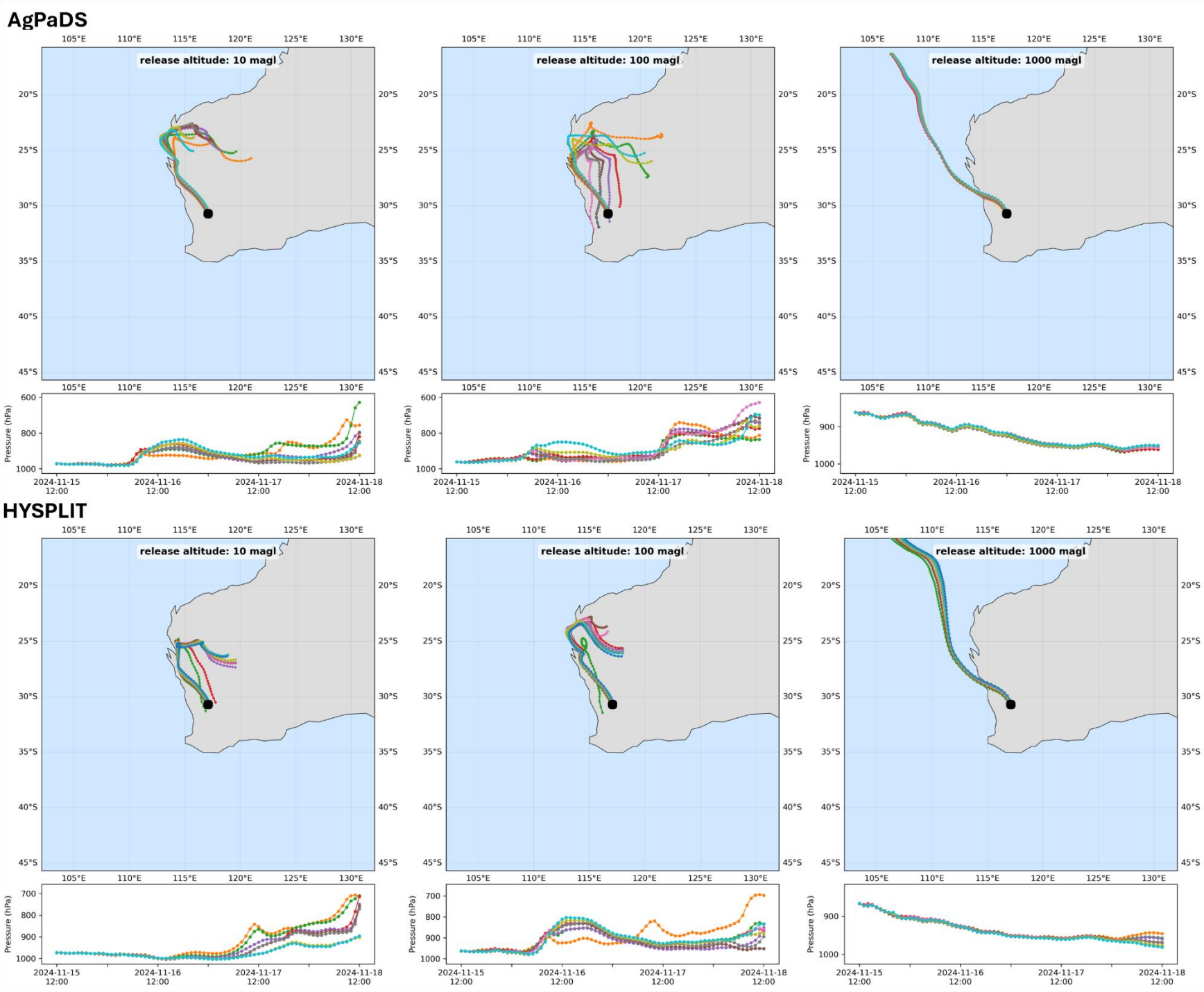

Figure S8: Comparison of stochastic Lagrangian particle modelling output computed by AgPaDS and HYSPLIT for a source in Australia

(a) top row: cumulative deposition at t=48h after release; bottom row: instantaneous particle plume in air at t=48h after release.

(b) deposition plume overlap.

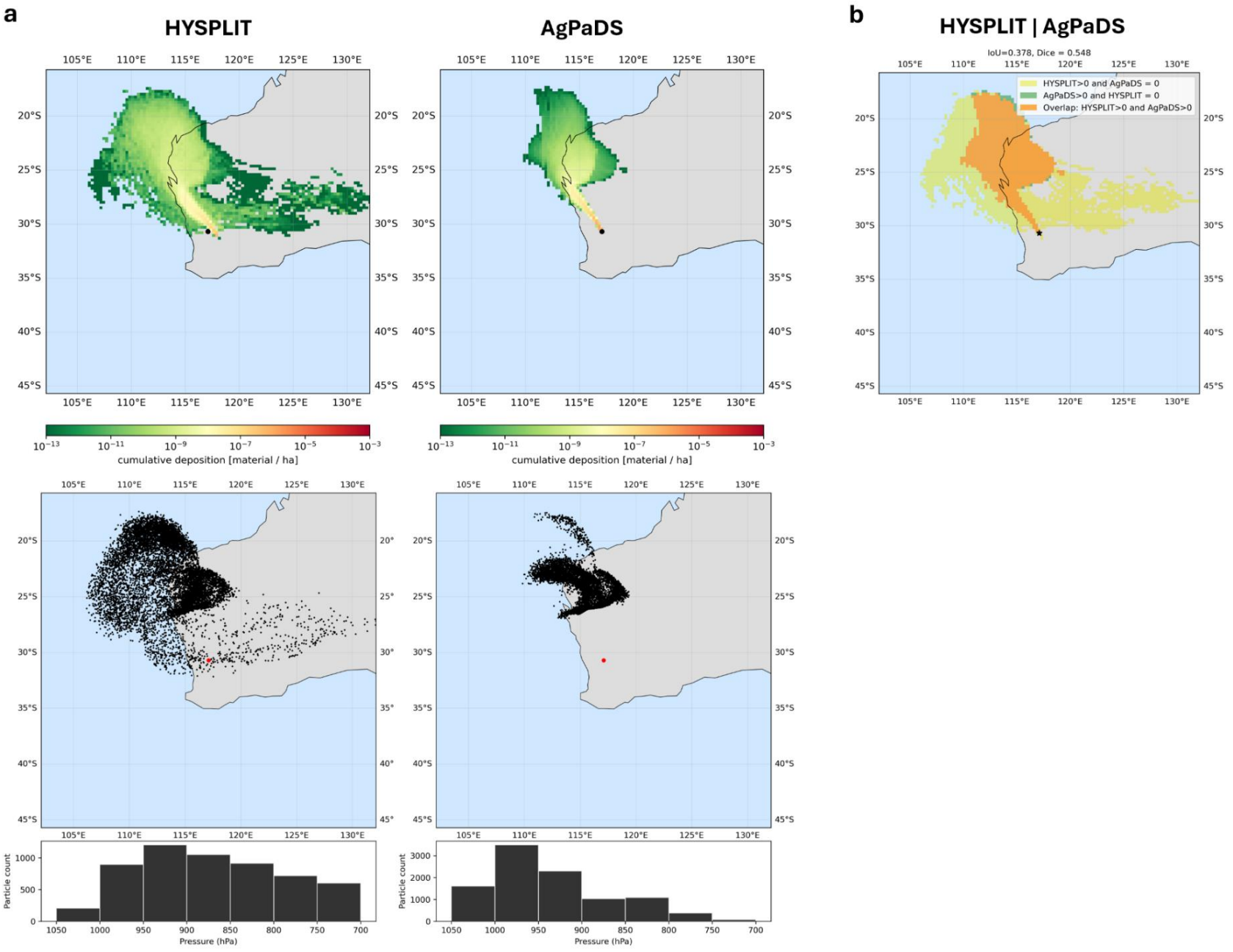

Figure S9: Comparison of mean trajectories computed by AgPaDS and HYSPLIT from a source in China at three different release altitudes

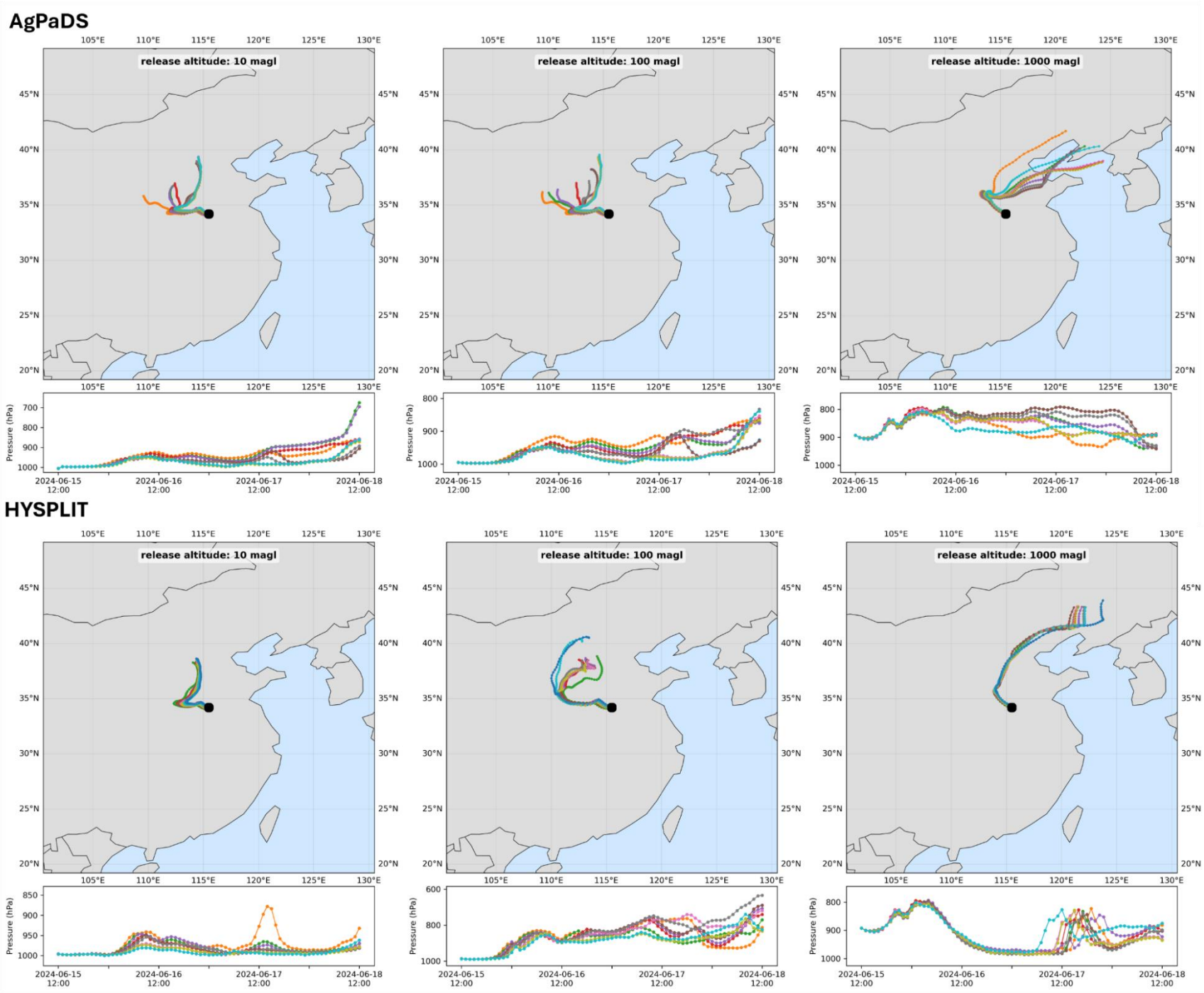

Figure S10: Comparison of stochastic Lagrangian particle modelling output computed by AgPaDS and HYSPLIT for a source in China

(a) top row: cumulative deposition at t=48h after release; bottom row: instantaneous particle plume in air at t=48h after release.

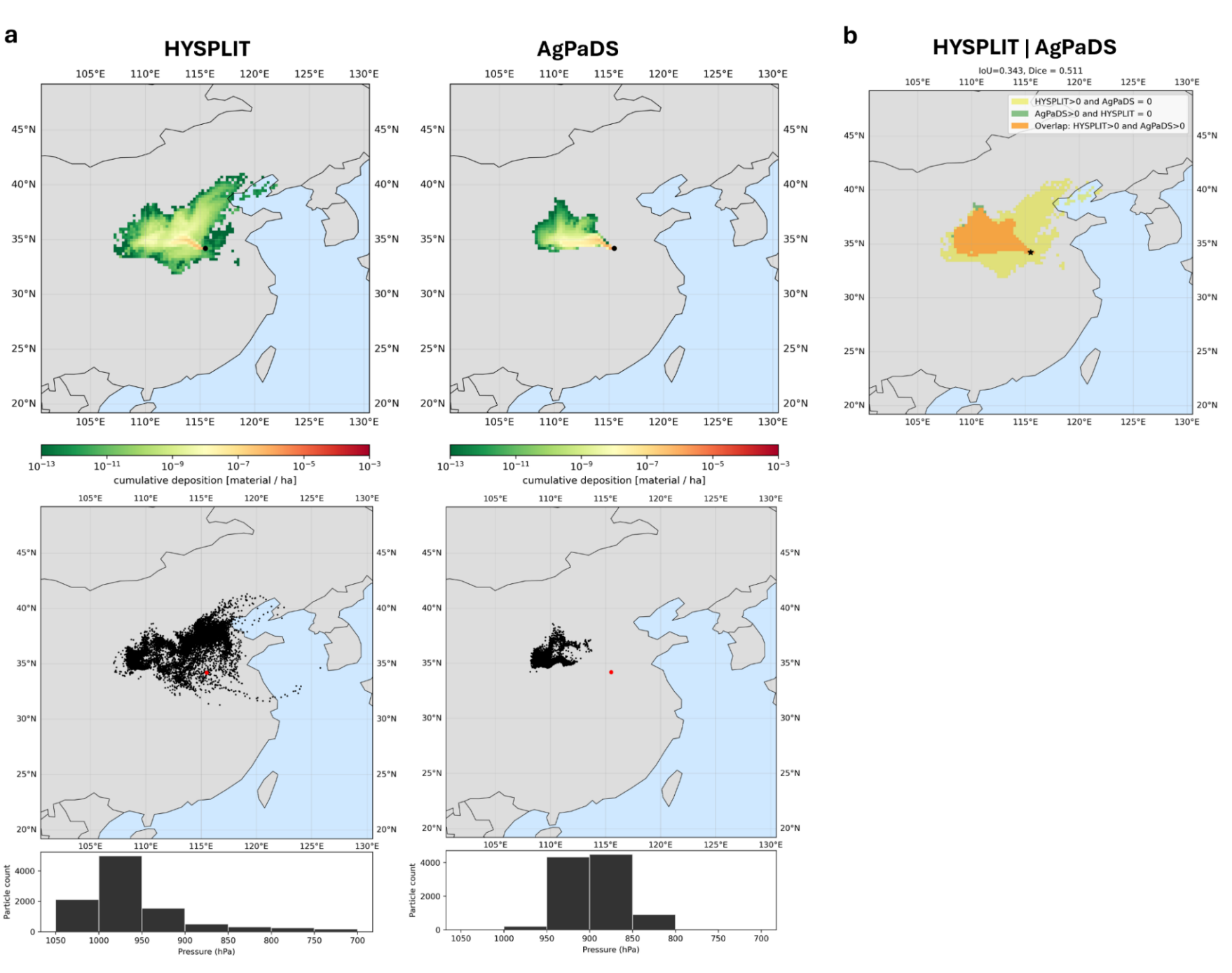

Figure S11: Comparison of mean trajectories computed by AgPaDS and HYSPLIT from a source in Denmark at three different release altitudes

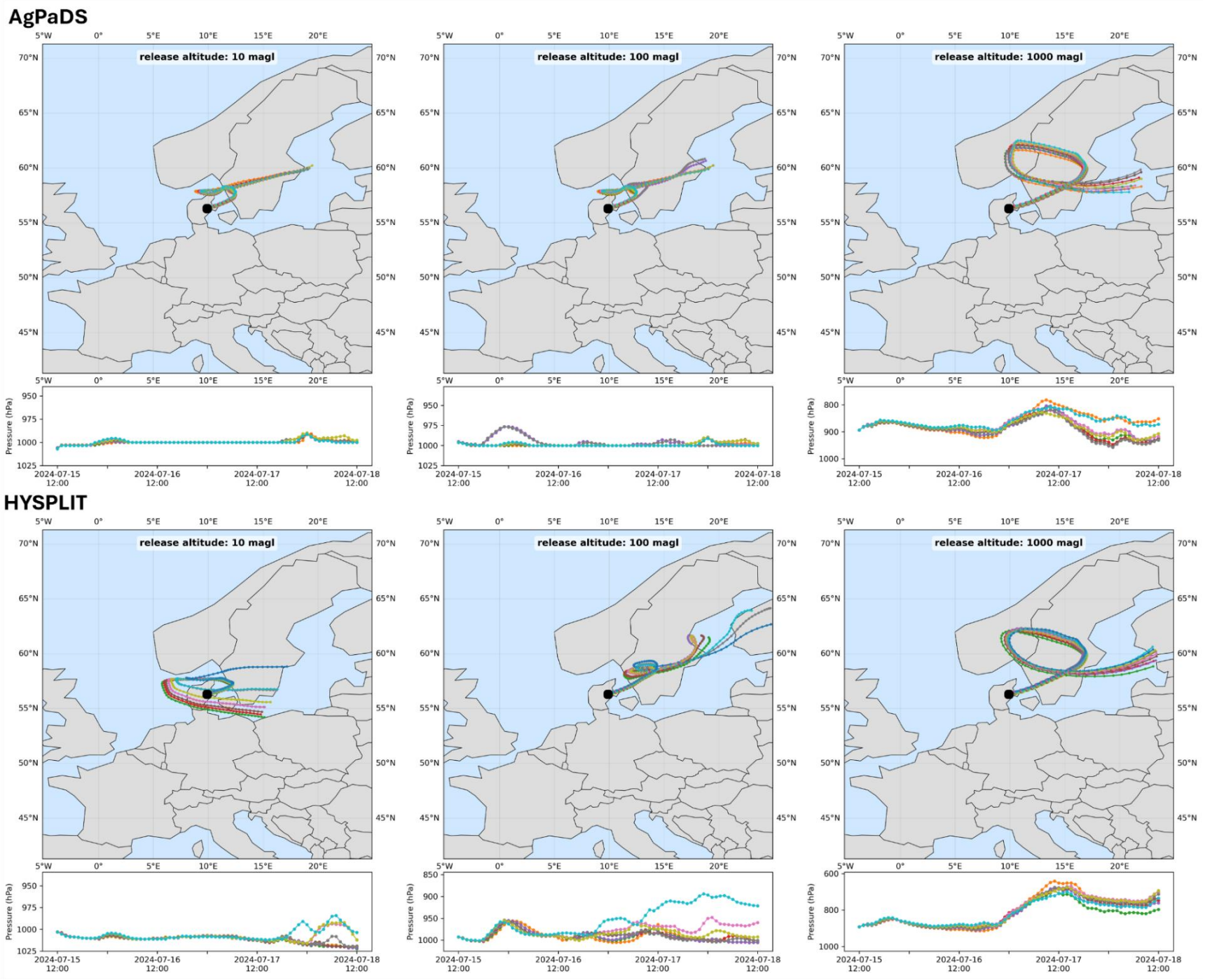

Figure S12: Comparison of stochastic Lagrangian particle modelling output computed by AgPaDS and HYSPLIT for a source in Denmark

(a) top row: cumulative deposition at t=48h after release; bottom row: instantaneous particle plume in air at t=48h after release.

(b) deposition plume overlap.

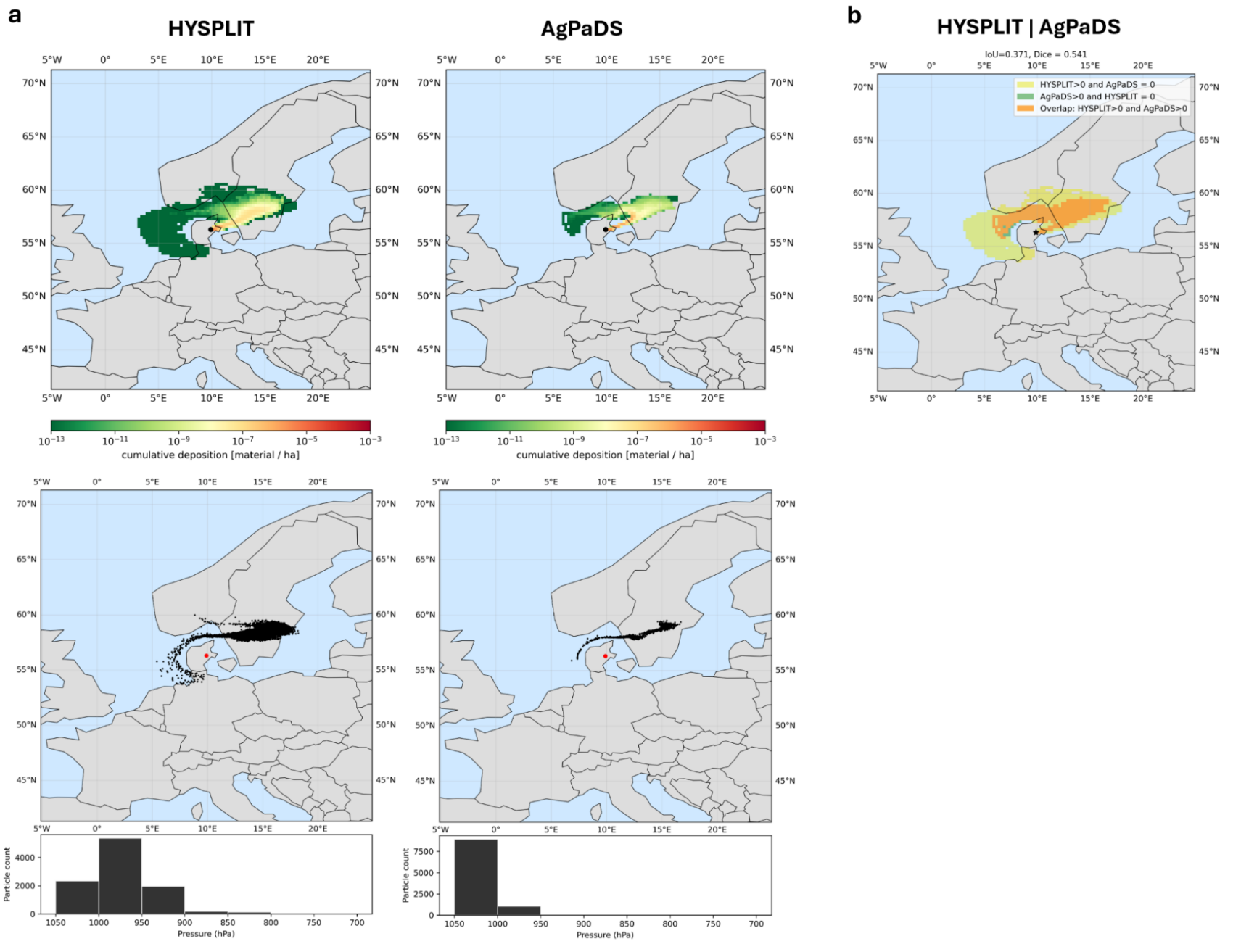

Figure S13: Comparison of mean trajectories computed by AgPaDS and HYSPLIT from a source in Ethiopia at three different release altitudes

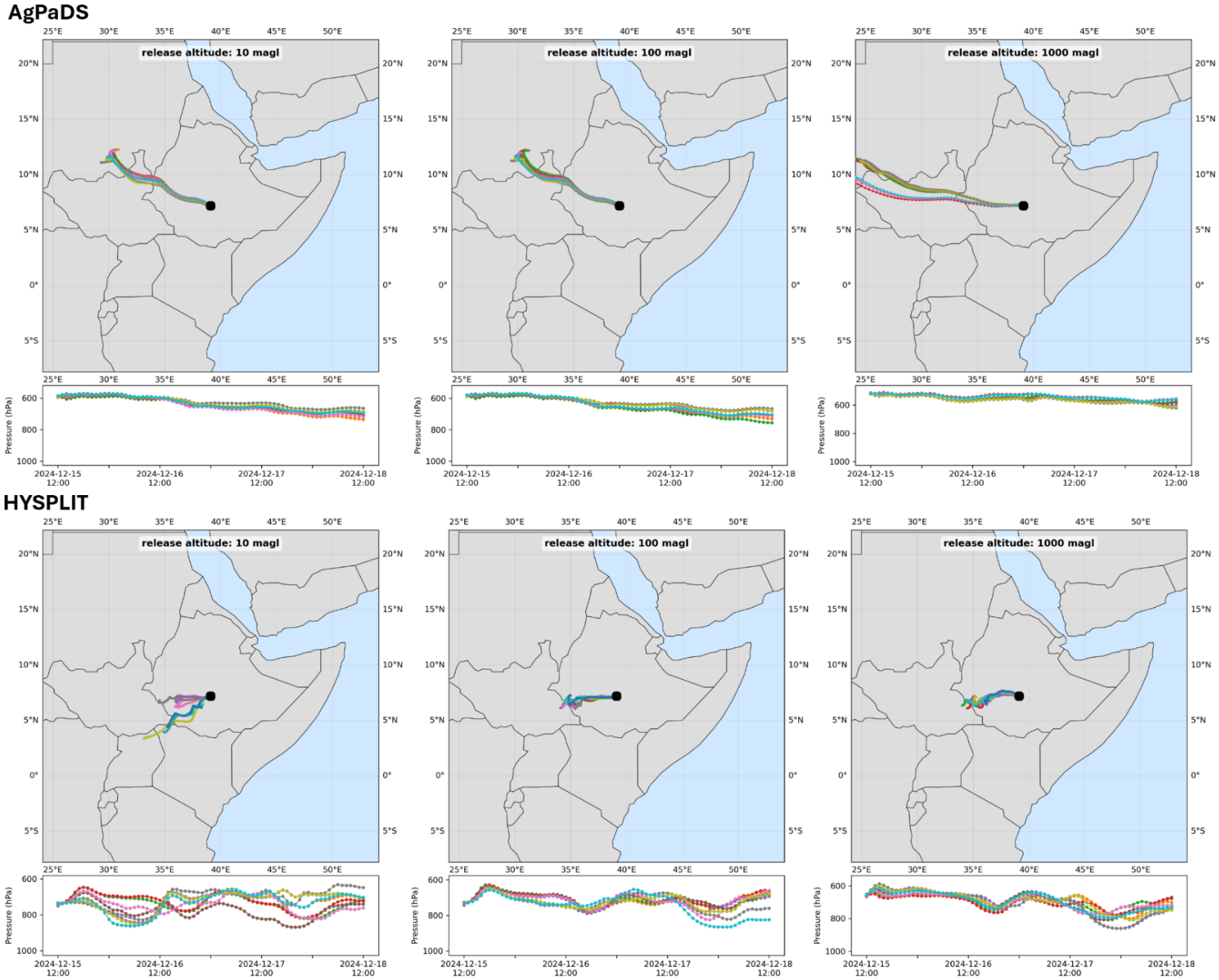

Figure S14: Comparison of stochastic Lagrangian particle modelling output computed by AgPaDS and HYSPLIT for a source in Ethiopia

(a) top row: cumulative deposition at t=48h after release; bottom row: instantaneous particle plume in air at t=48h after release.

(b) deposition plume overlap.

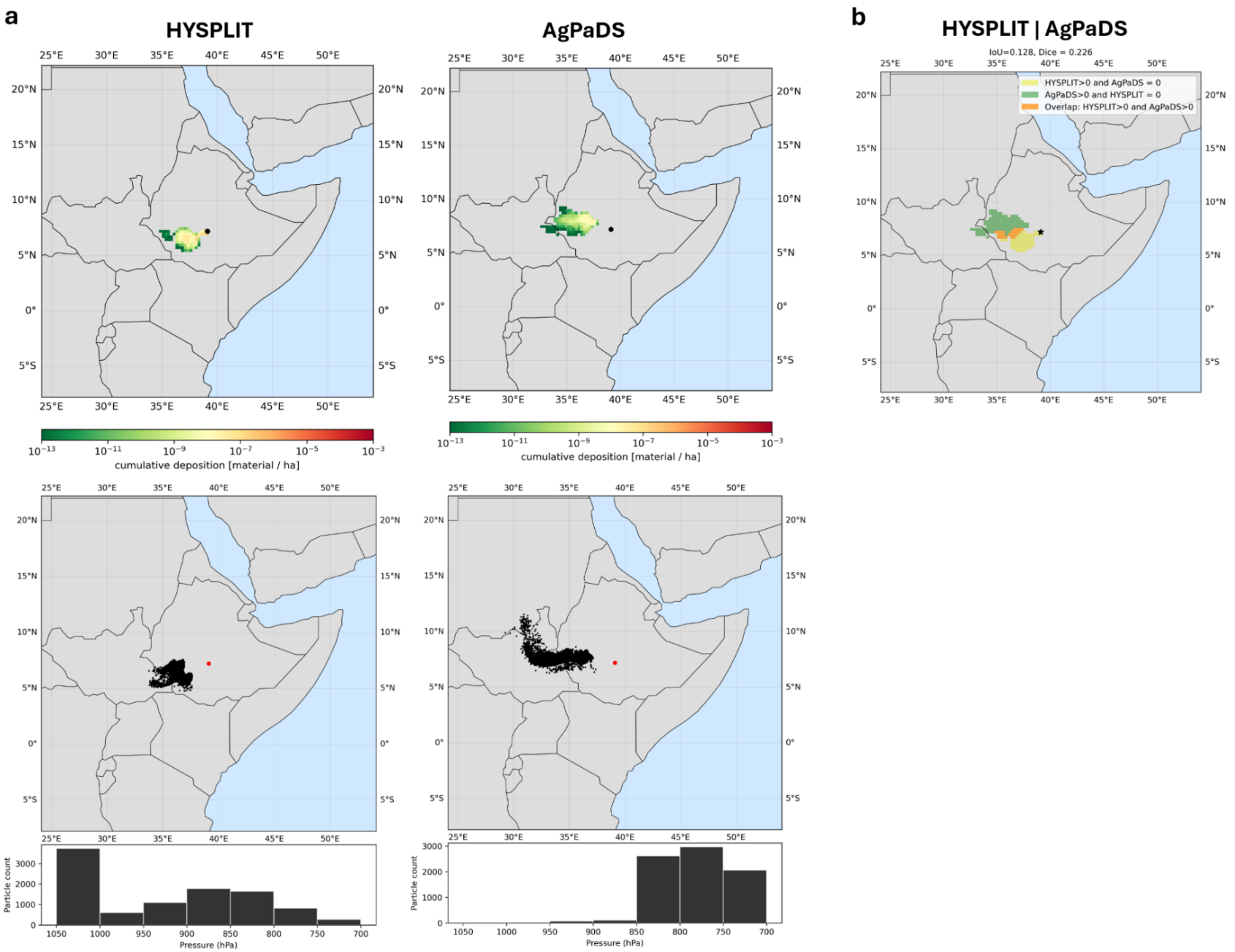

Figure S15: Comparison of mean trajectories computed by AgPaDS and HYSPLIT from a source in India at three different release altitudes

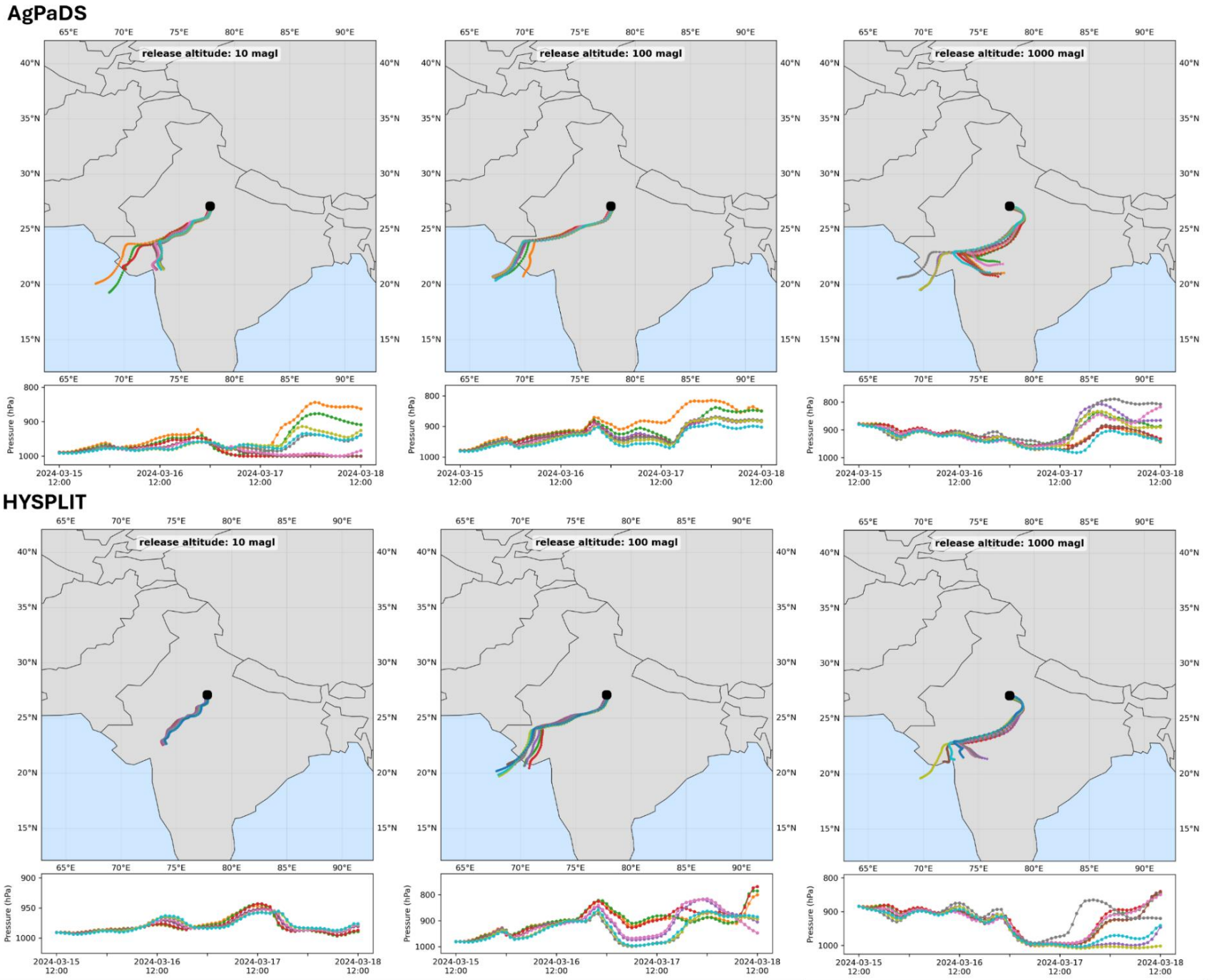

Figure S16: Comparison of stochastic Lagrangian particle modelling output computed by AgPaDS and HYSPLIT for a source in India

(a) top row: cumulative deposition at t=48h after release; bottom row: instantaneous particle plume in air at t=48h after release.

(b) deposition plume overlap.

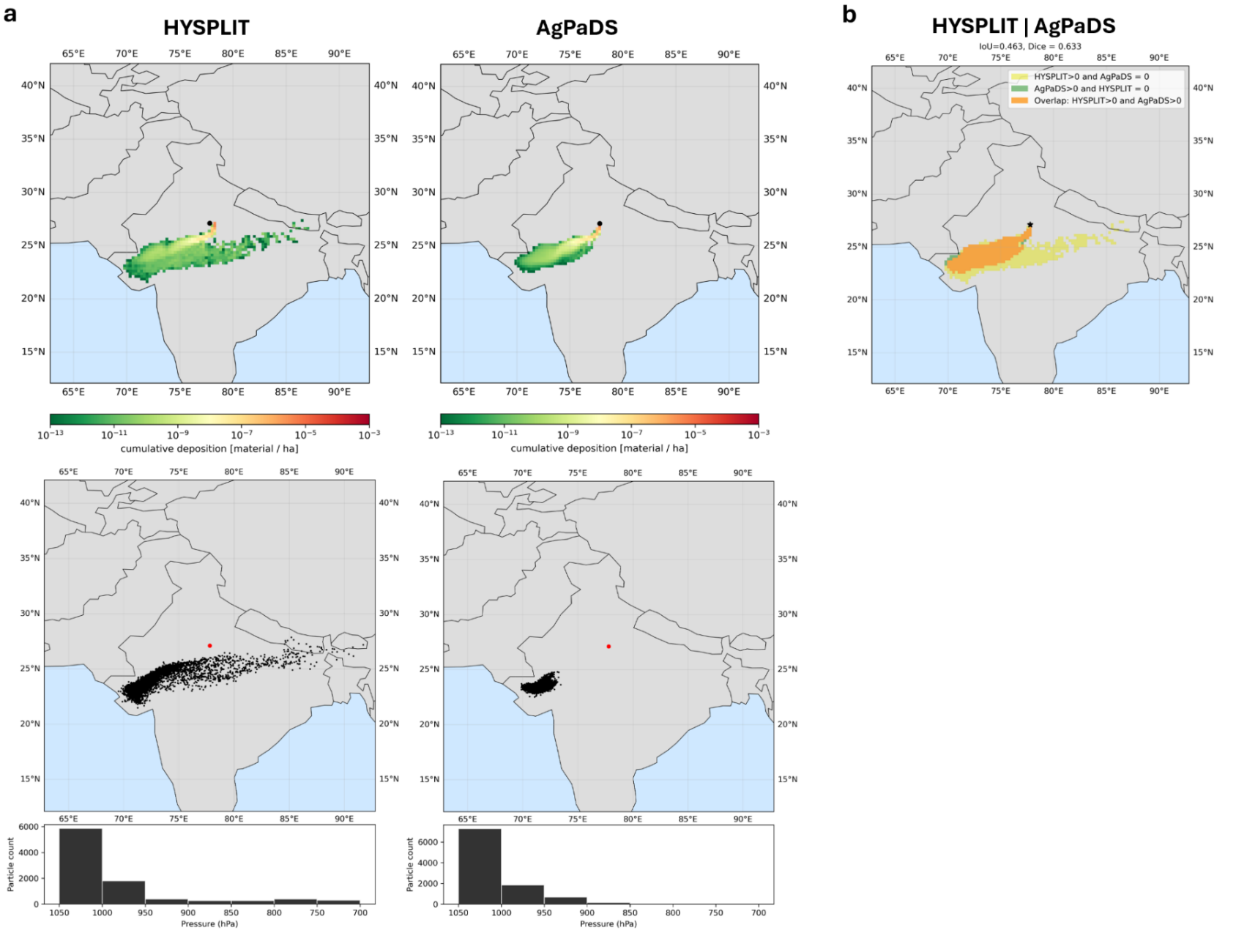

Figure S17: Comparison of mean trajectories computed by AgPaDS and HYSPLIT from a source in Iran at three different release altitudes

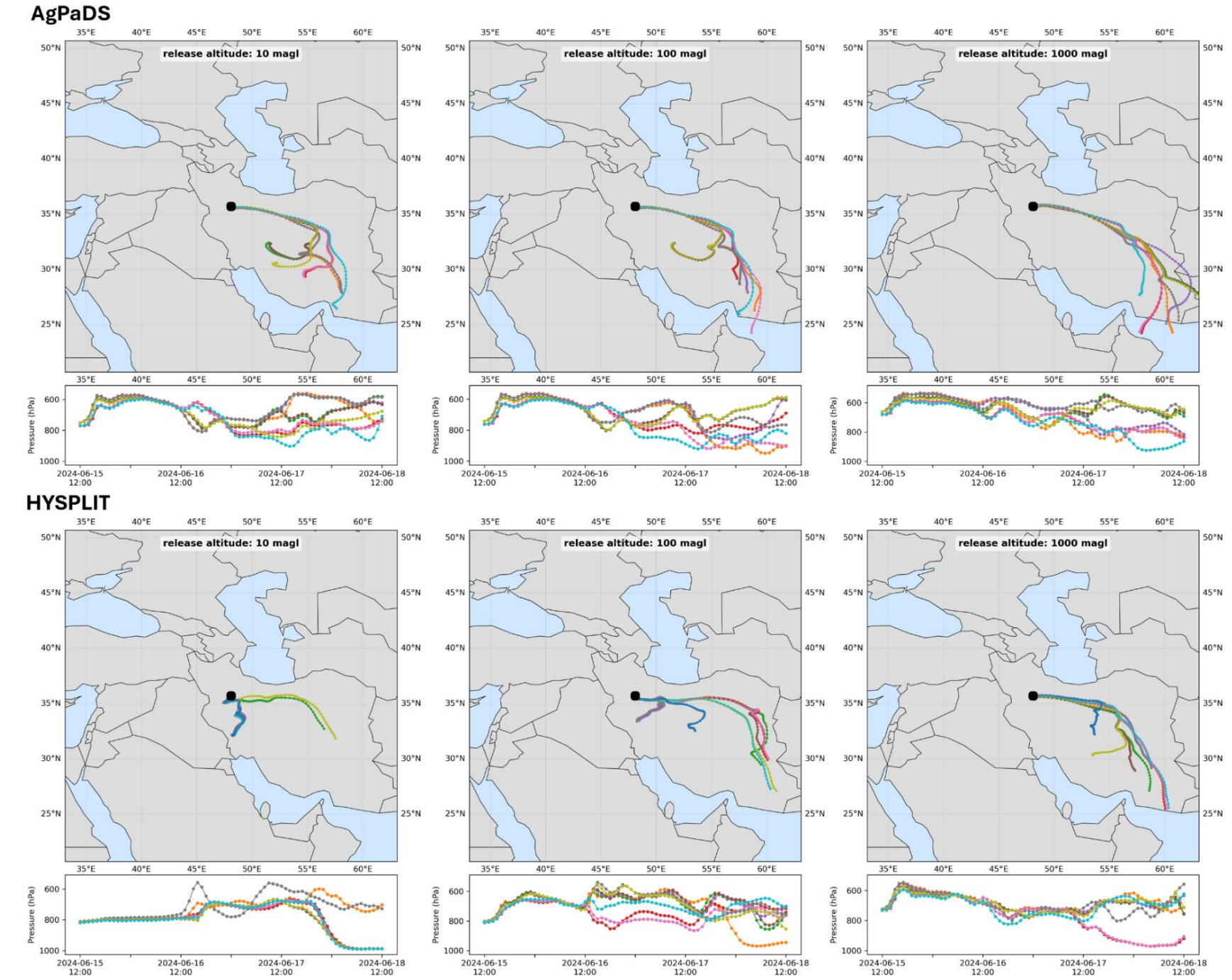

Figure S18: Comparison of stochastic Lagrangian particle modelling output computed by AgPaDS and HYSPLIT for a source in Iran

(a) top row: cumulative deposition at t=48h after release; bottom row: instantaneous particle plume in air at t=48h after release.

(b) deposition plume overlap.

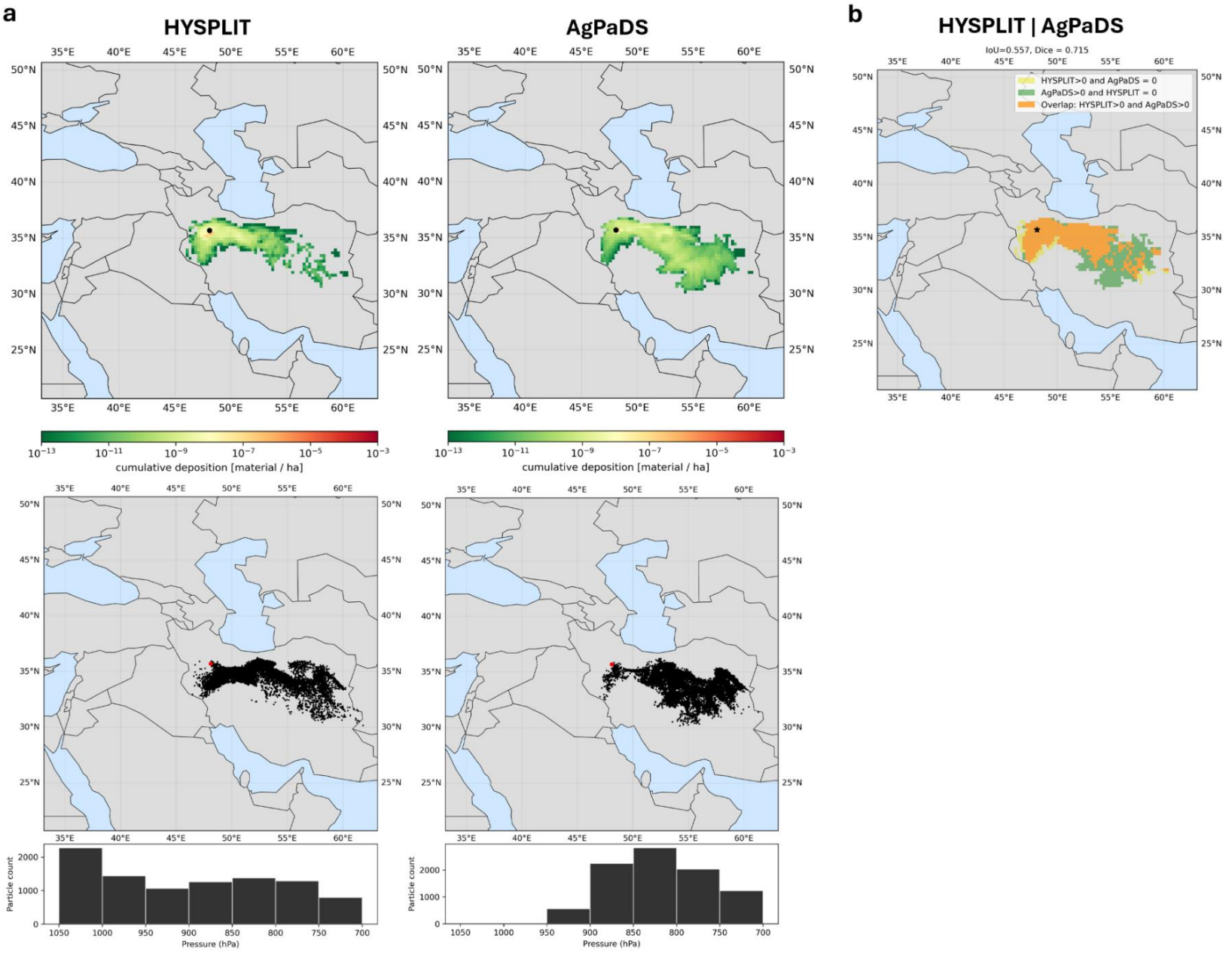

Figure S19: Comparison of mean trajectories computed by AgPaDS and HYSPLIT from a source in Italy at three different release altitudes

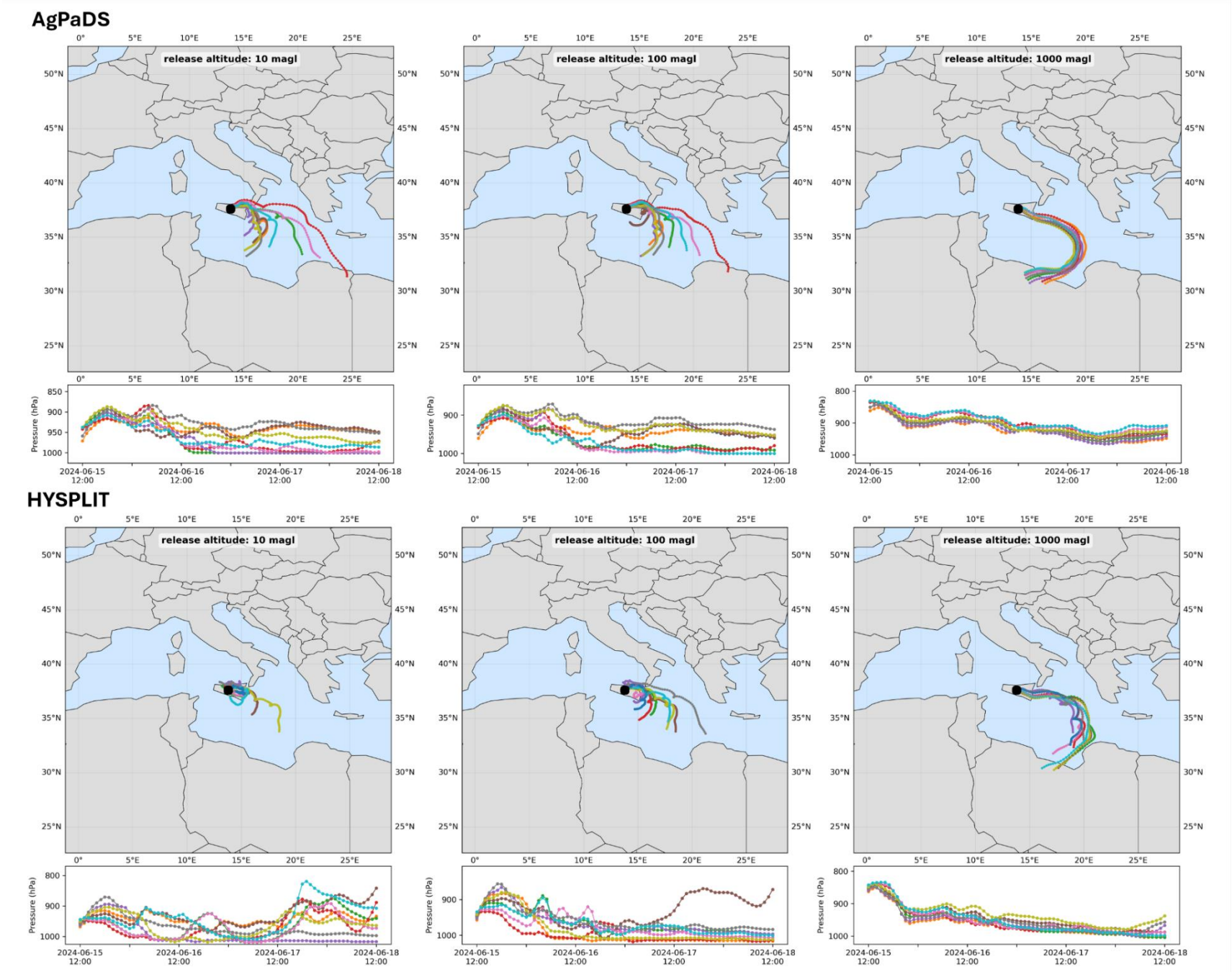

Figure S20: Comparison of stochastic Lagrangian particle modelling output computed by AgPaDS and HYSPLIT for a source in Italy

(a) top row: cumulative deposition at t=48h after release; bottom row: instantaneous particle plume in air at t=48h after release.

(b) deposition plume overlap.

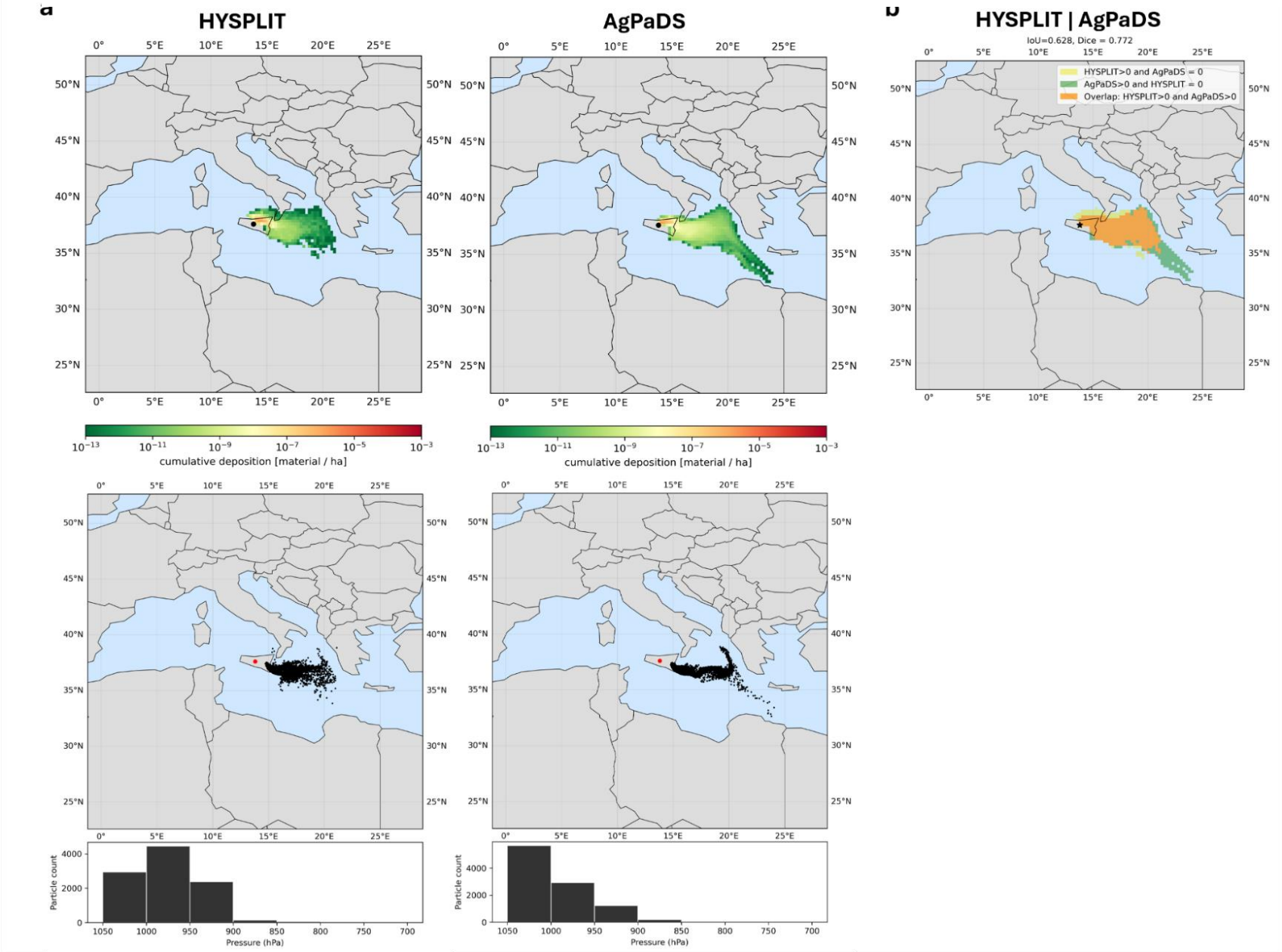

Figure S21: Comparison of mean trajectories computed by AgPaDS and HYSPLIT from a source in Kazakhstan at three different release altitudes

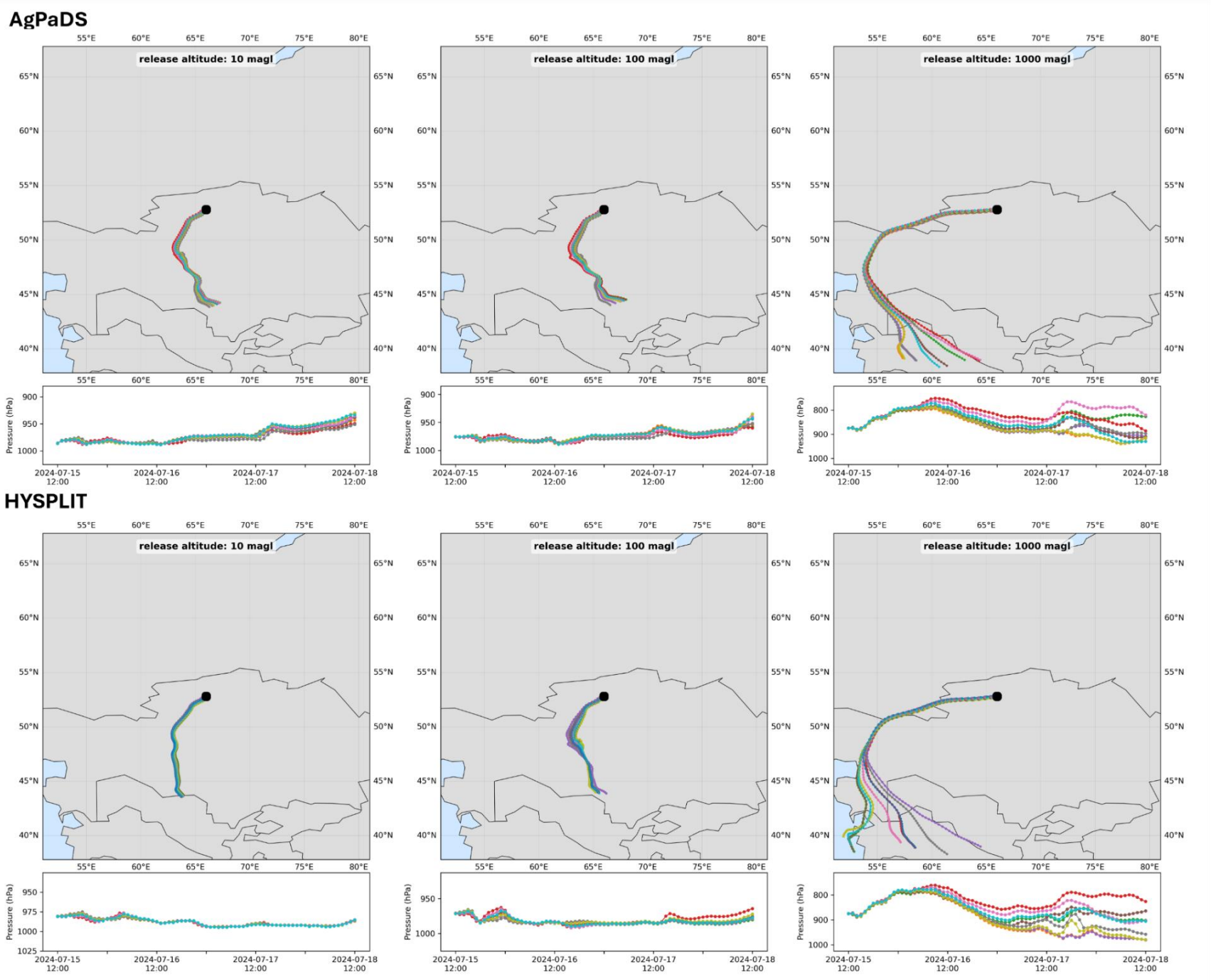

Figure S22: Comparison of stochastic Lagrangian particle modelling output computed by AgPaDS and HYSPLIT for a source in Kazakhstan

(a) top row: cumulative deposition at t=48h after release; bottom row: instantaneous particle plume in air at t=48h after release.

(b) deposition plume overlap.

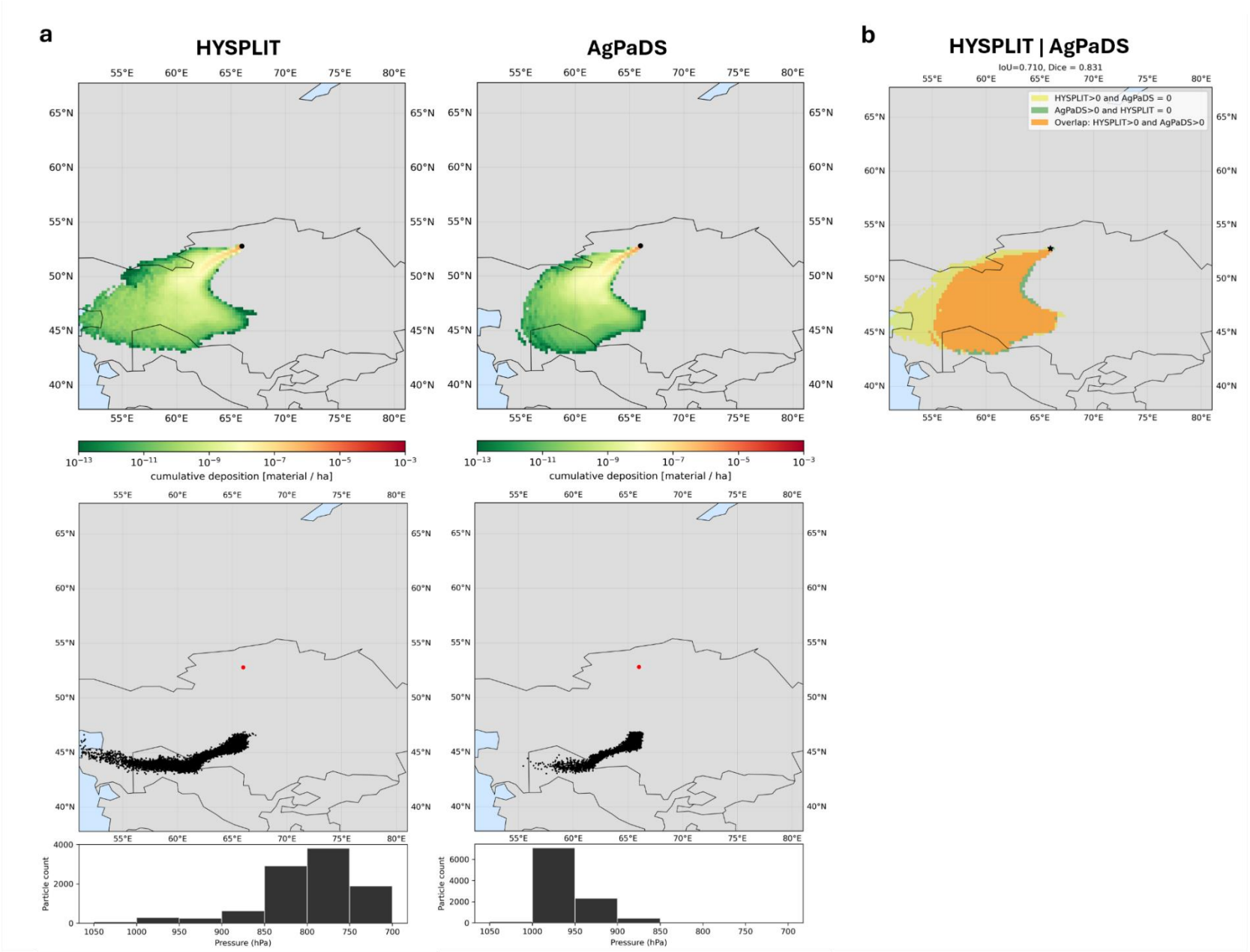

Figure S23: Comparison of mean trajectories computed by AgPaDS and HYSPLIT from a source in Morocco at three different release altitudes

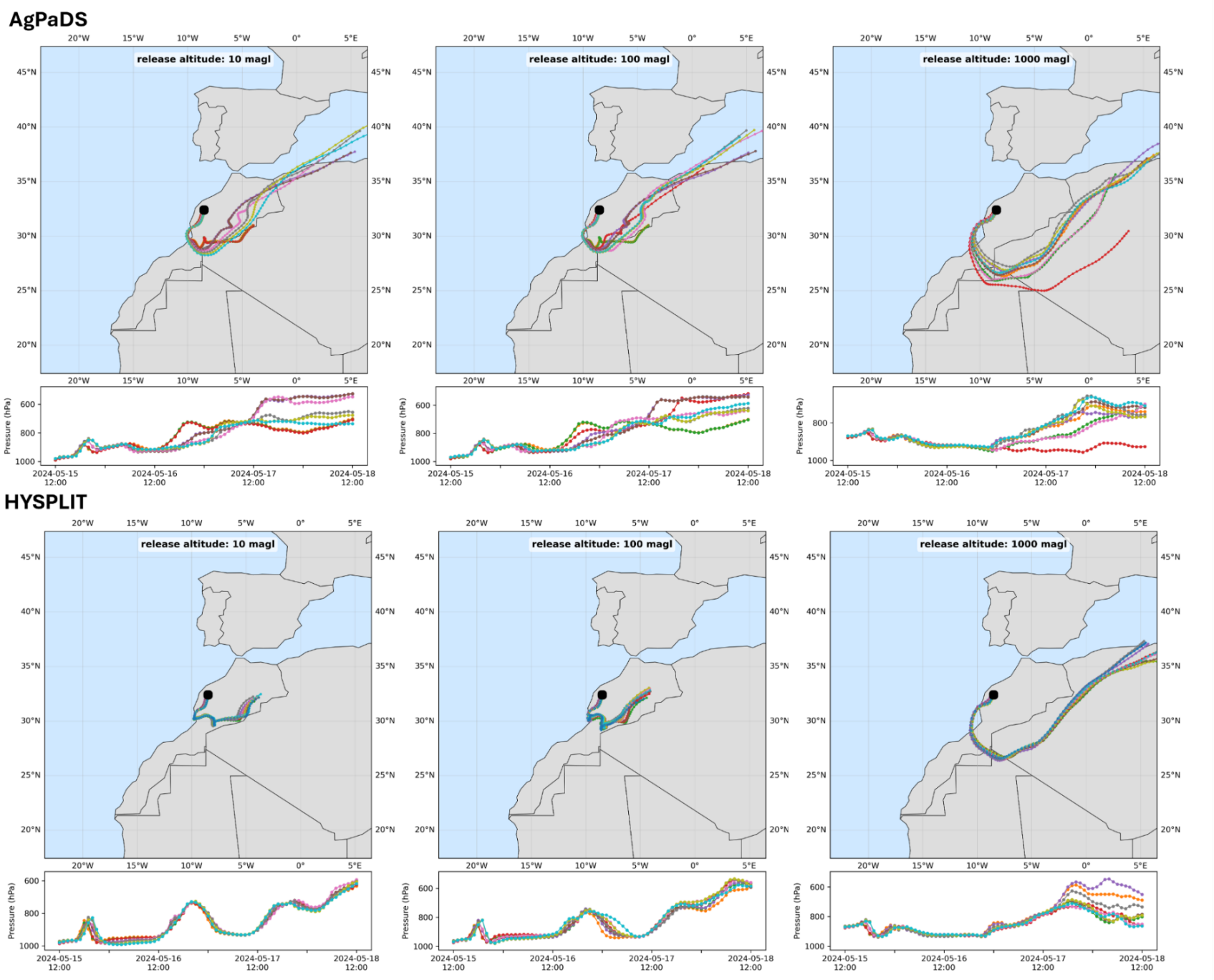

Figure S24: Comparison of stochastic Lagrangian particle modelling output computed by AgPaDS and HYSPLIT for a source in Morocco

(a) top row: cumulative deposition at t=48h after release; bottom row: instantaneous particle plume in air at t=48h after release.

(b) deposition plume overlap.

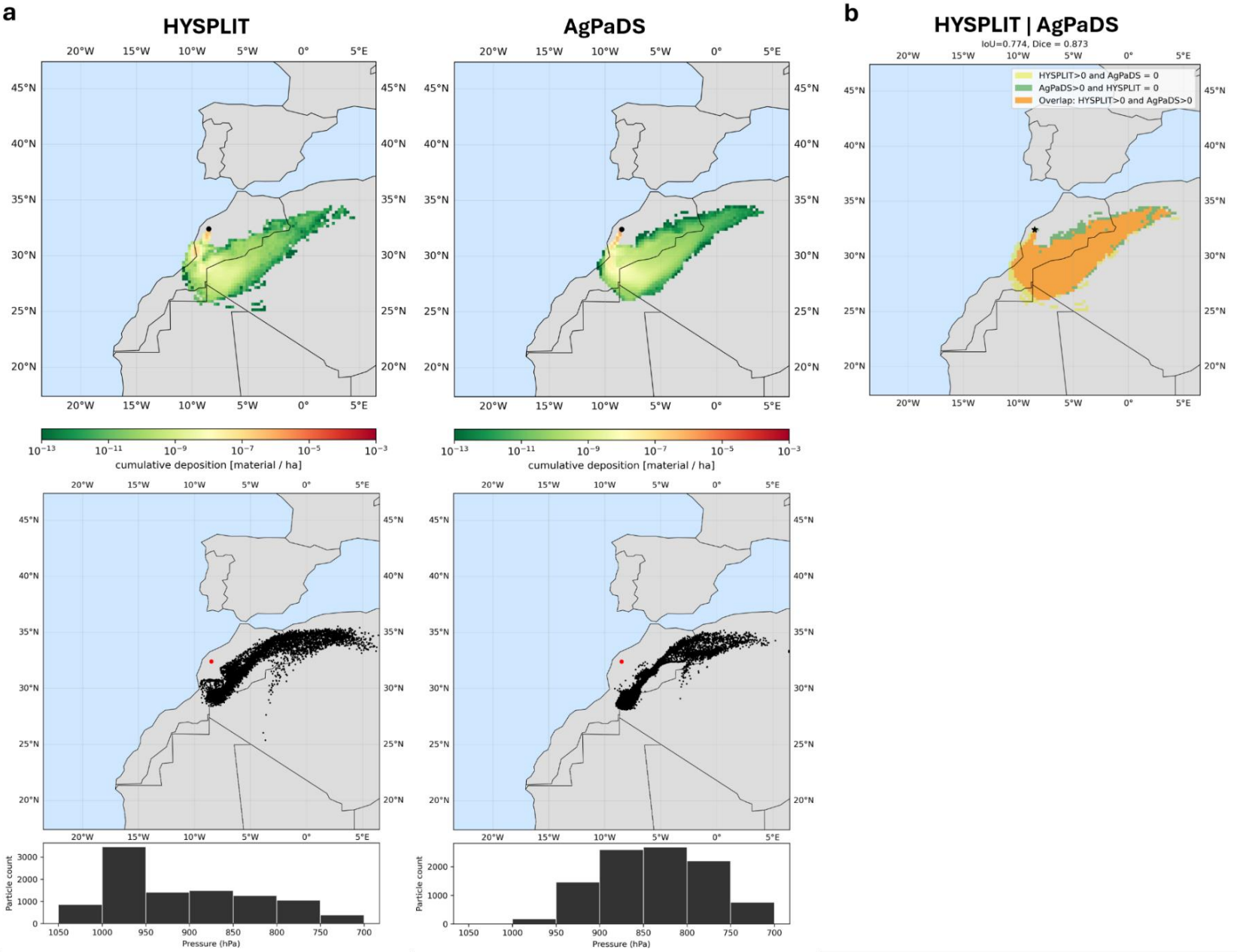

Figure S25: Comparison of mean trajectories computed by AgPaDS and HYSPLIT from a source in Mexico at three different release altitudes

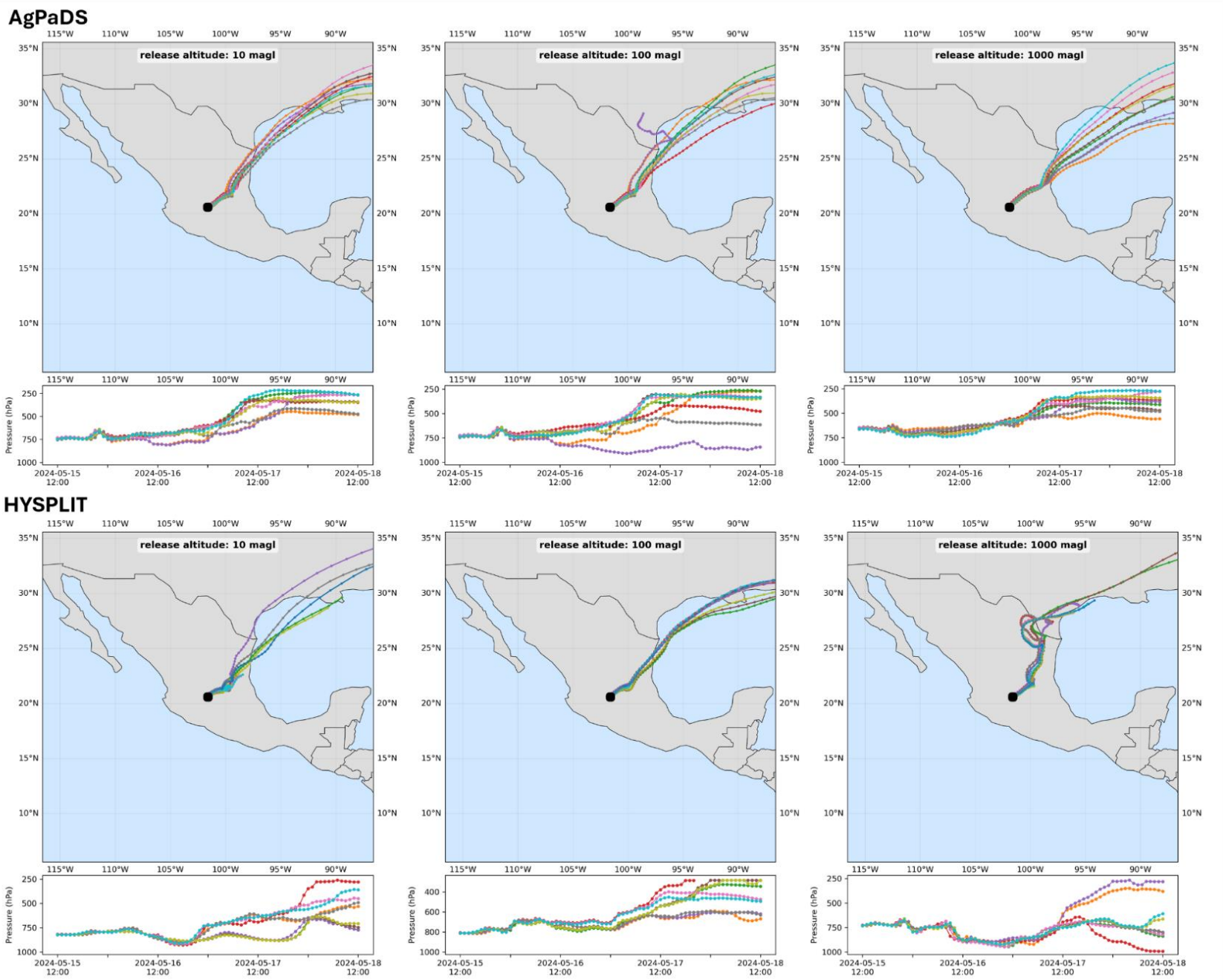

Figure S26: Comparison of stochastic Lagrangian particle modelling output computed by AgPaDS and HYSPLIT for a source in Mexico

(a) top row: cumulative deposition at t=48h after release; bottom row: instantaneous particle plume in air at t=48h after release.

(b) deposition plume overlap.

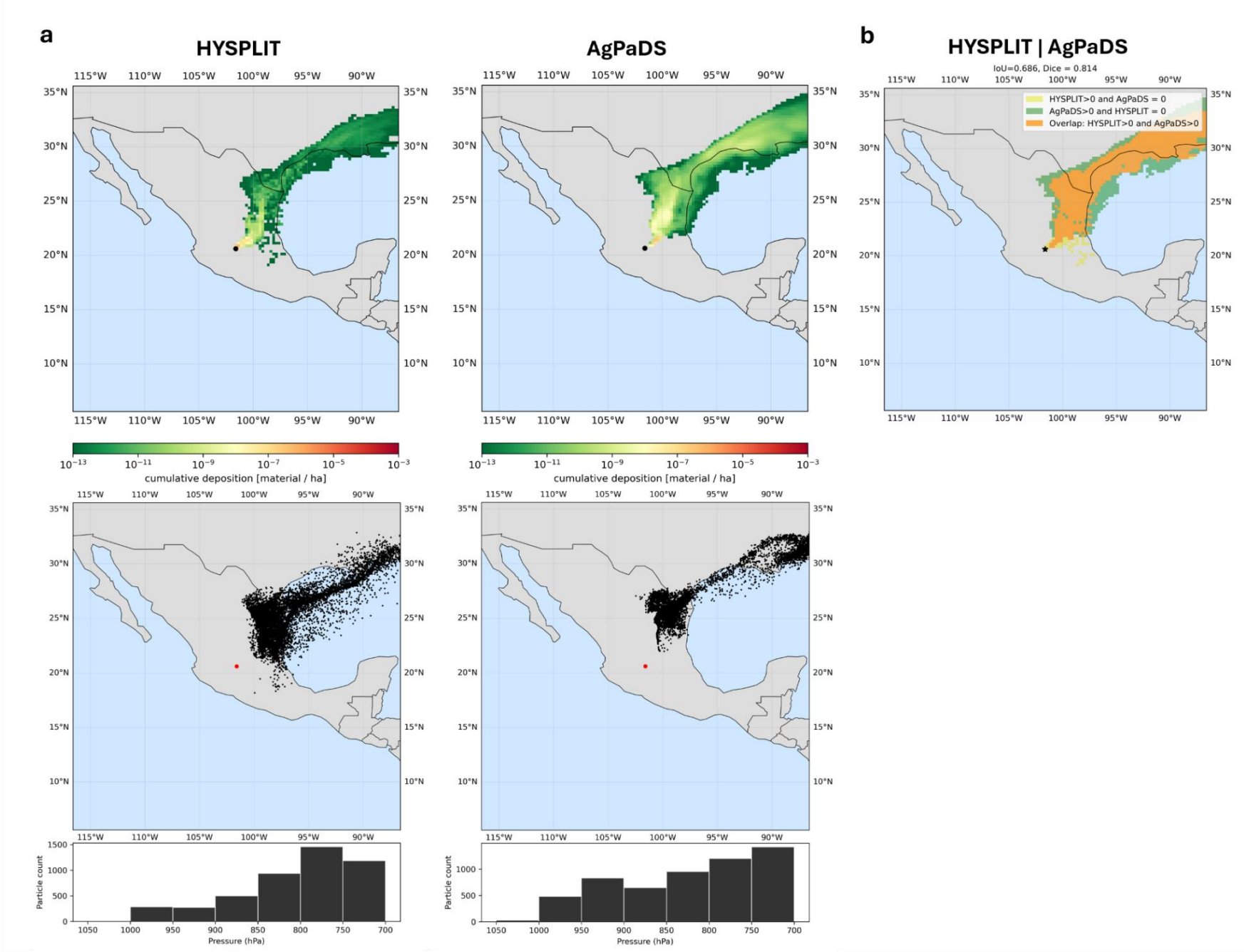

Figure S27: Comparison of mean trajectories computed by AgPaDS and HYSPLIT from a source in Pakistan at three different release altitudes

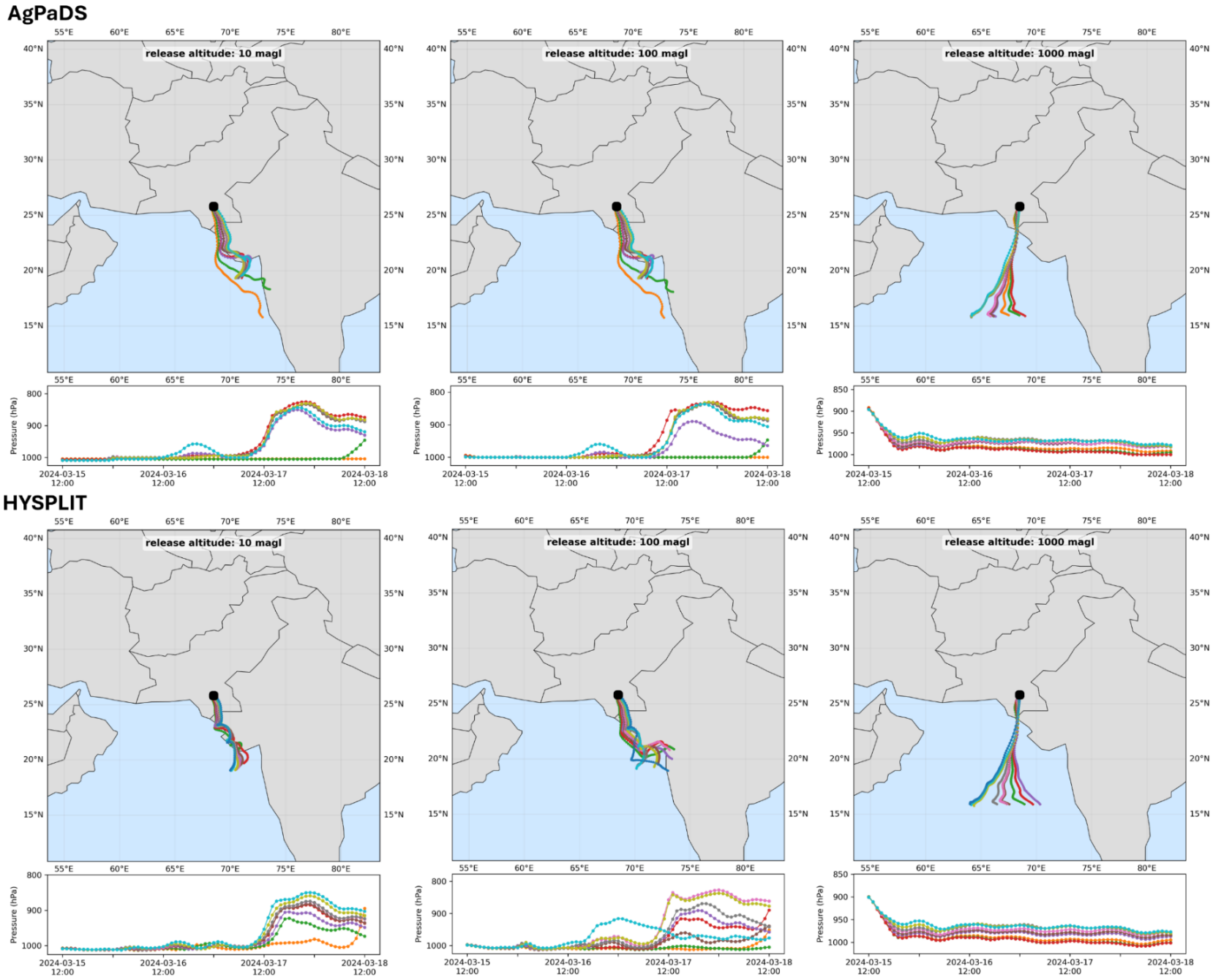

Figure S28: Comparison of stochastic Lagrangian particle modelling output computed by AgPaDS and HYSPLIT for a source in Pakistan

(a) top row: cumulative deposition at t=48h after release; bottom row: instantaneous particle plume in air at t=48h after release.

(b) deposition plume overlap.

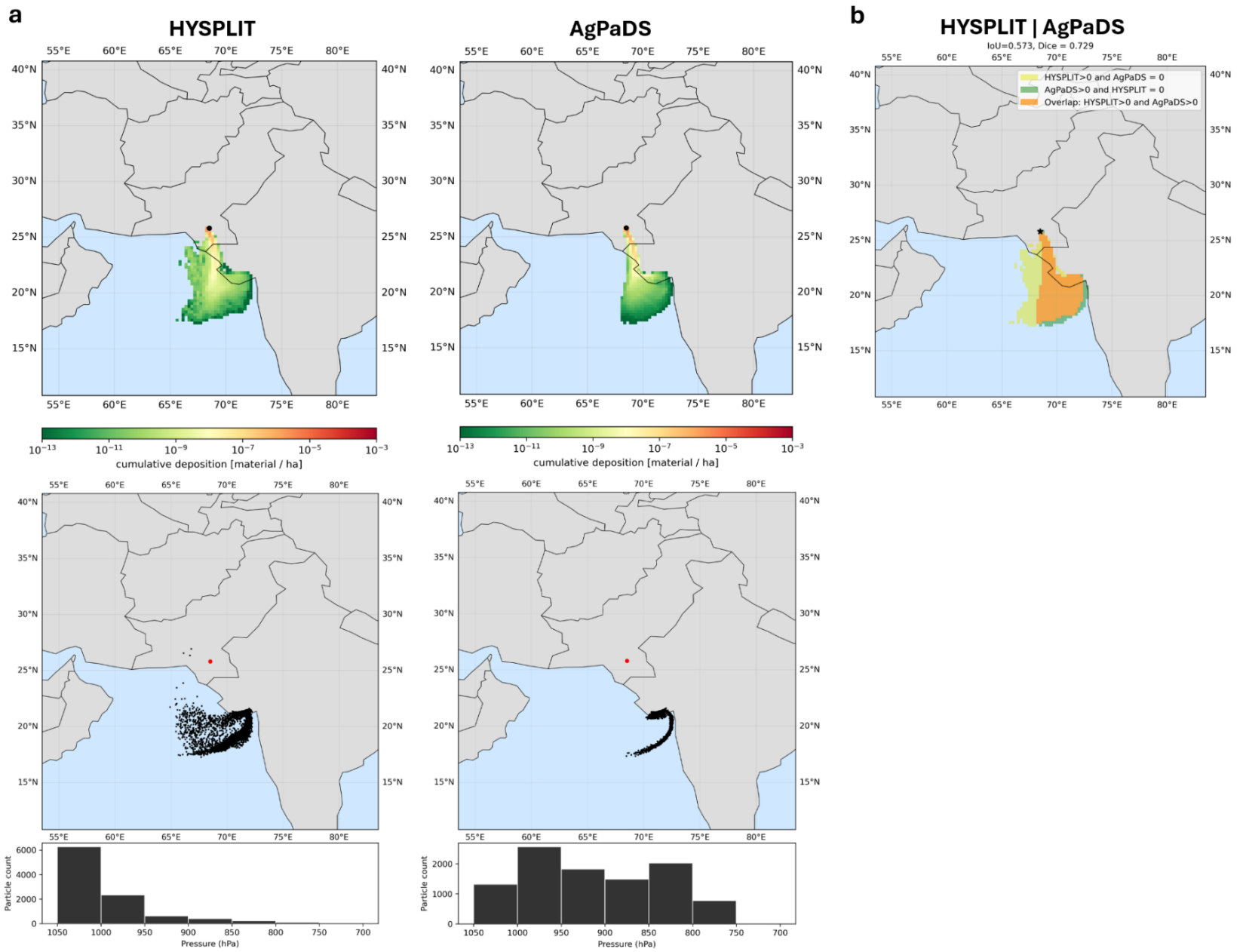

Figure S29: Comparison of mean trajectories computed by AgPaDS and HYSPLIT from a source in Russia at three different release altitudes

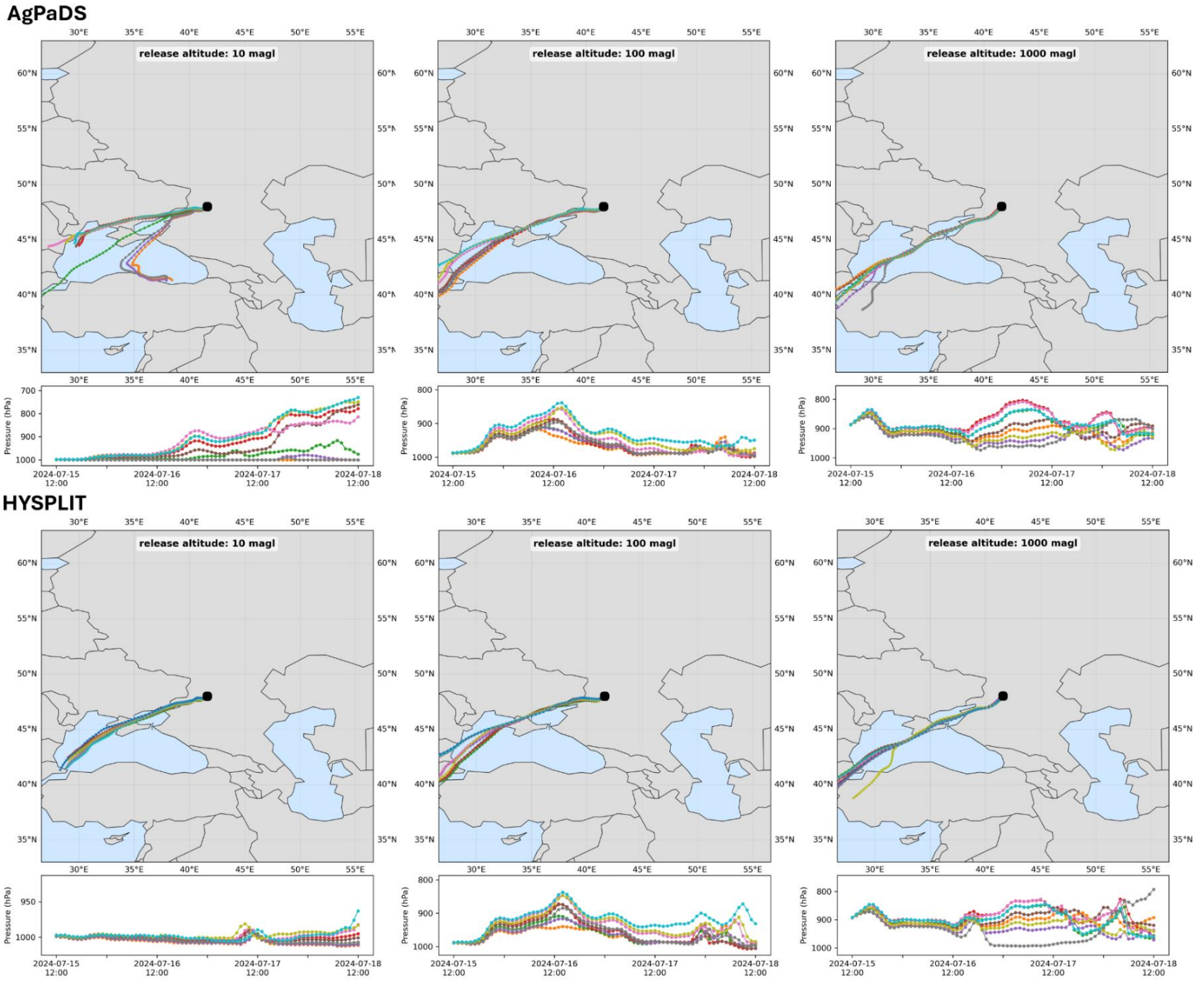

Figure S30: Comparison of stochastic Lagrangian particle modelling output computed by AgPaDS and HYSPLIT for a source in Russia

(a) top row: cumulative deposition at t=48h after release; bottom row: instantaneous particle plume in air at t=48h after release.

(b) deposition plume overlap.

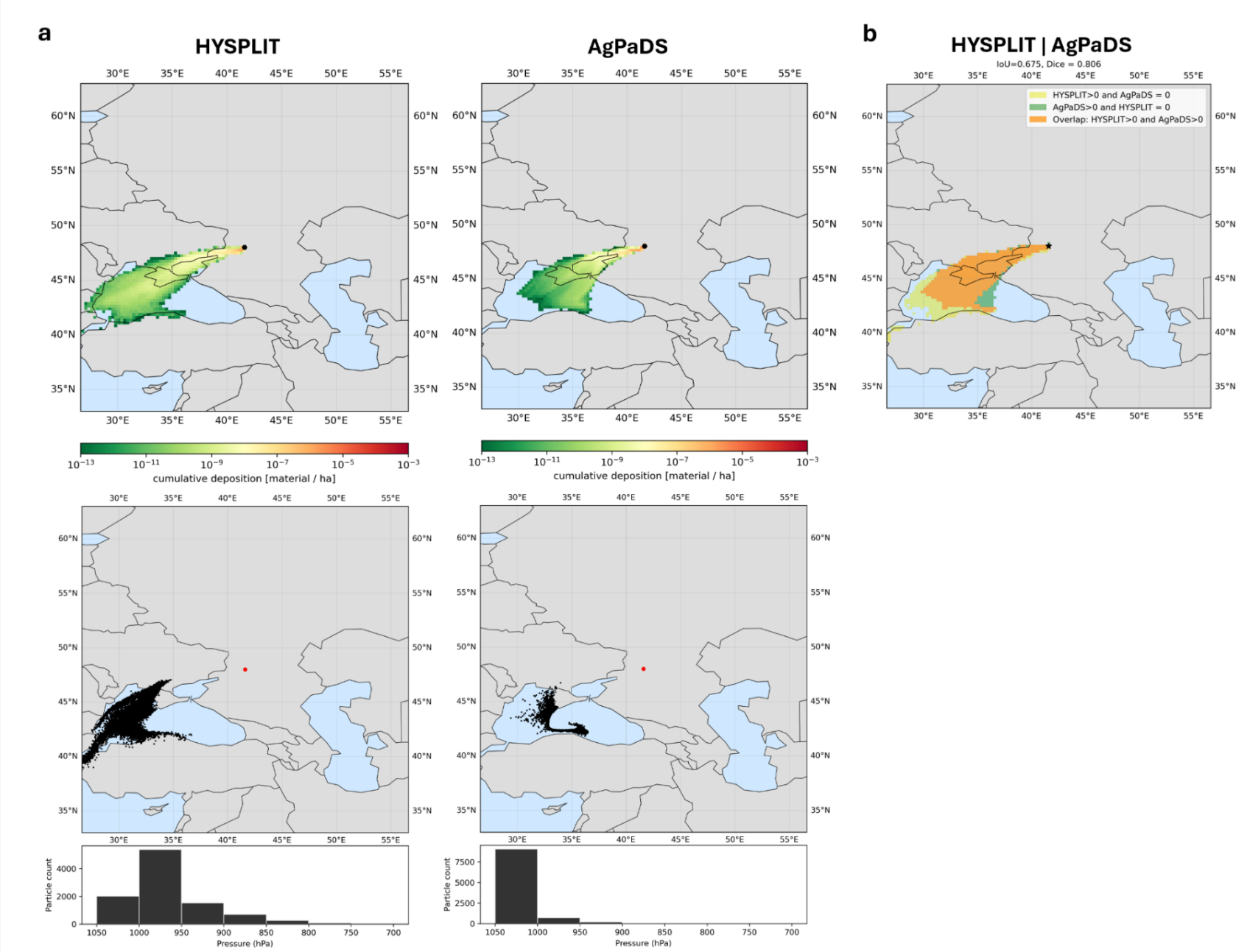

Figure S31: Comparison of mean trajectories computed by AgPaDS and HYSPLIT from a source in South-Africa at three different release altitudes.

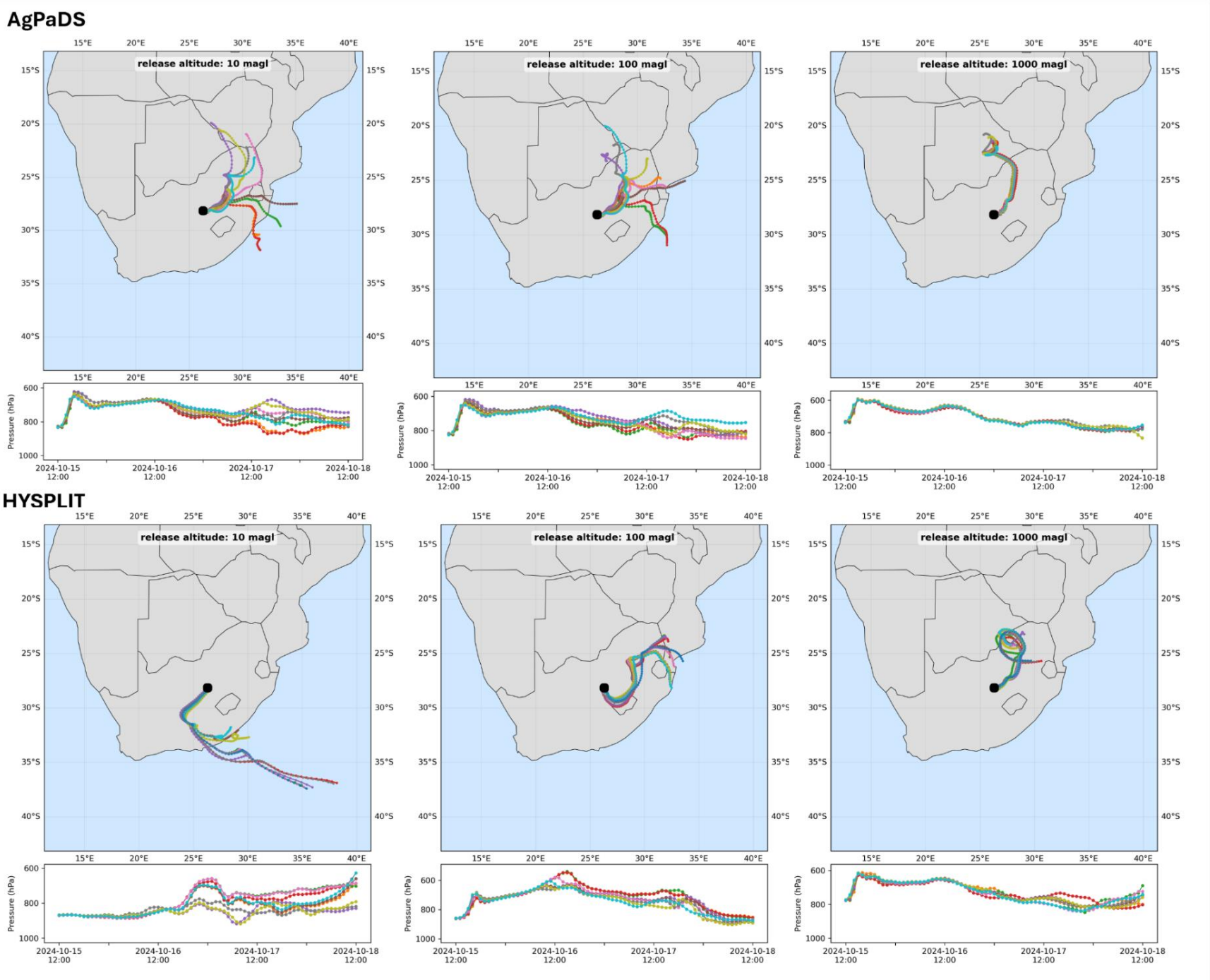

Figure S32: Comparison of stochastic Lagrangian particle modelling output computed by AgPaDS and HYSPLIT for a source in South-Africa

(a) top row: cumulative deposition at t=48h after release; bottom row: instantaneous particle plume in air at t=48h after release.

(b) deposition plume overlap.

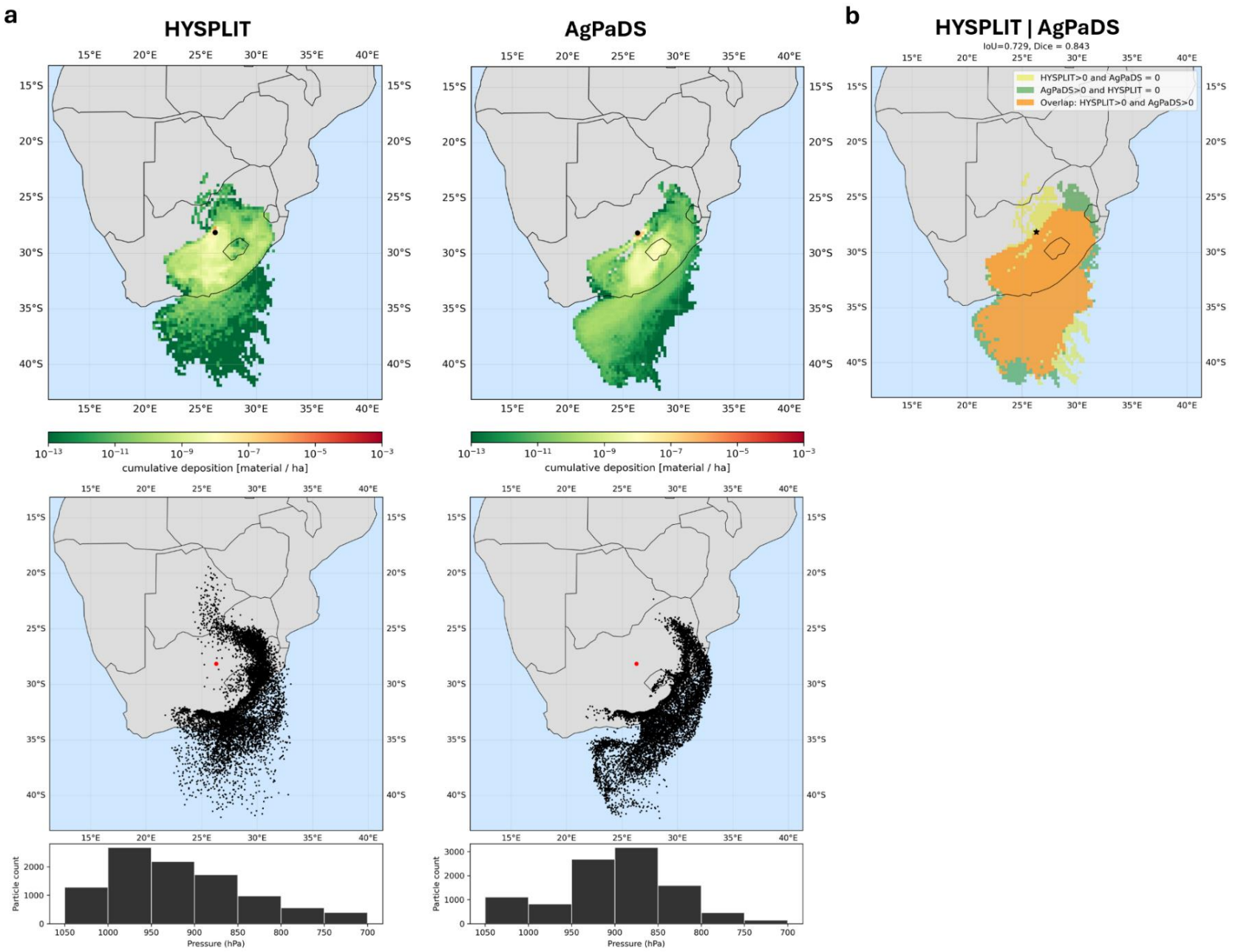

Figure S33: Comparison of mean trajectories computed by AgPaDS and HYSPLIT from a source in USA at three different release altitudes.

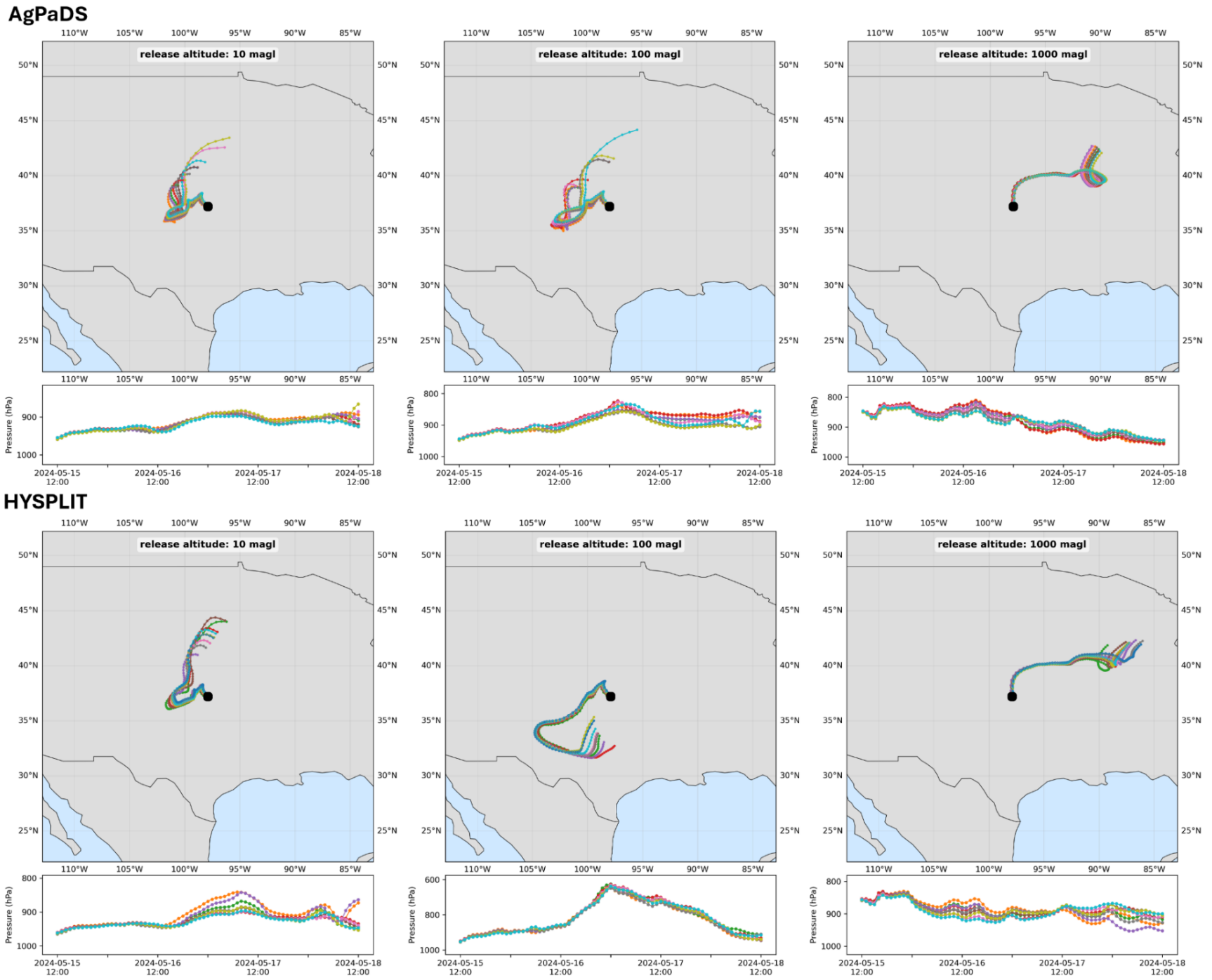

Figure S34: Comparison of stochastic Lagrangian particle modelling output computed by AgPaDS and HYSPLIT for a source in USA

(a) top row: cumulative deposition at t=48h after release; bottom row: instantaneous particle plume in air at t=48h after release.

(b) deposition plume overlap.

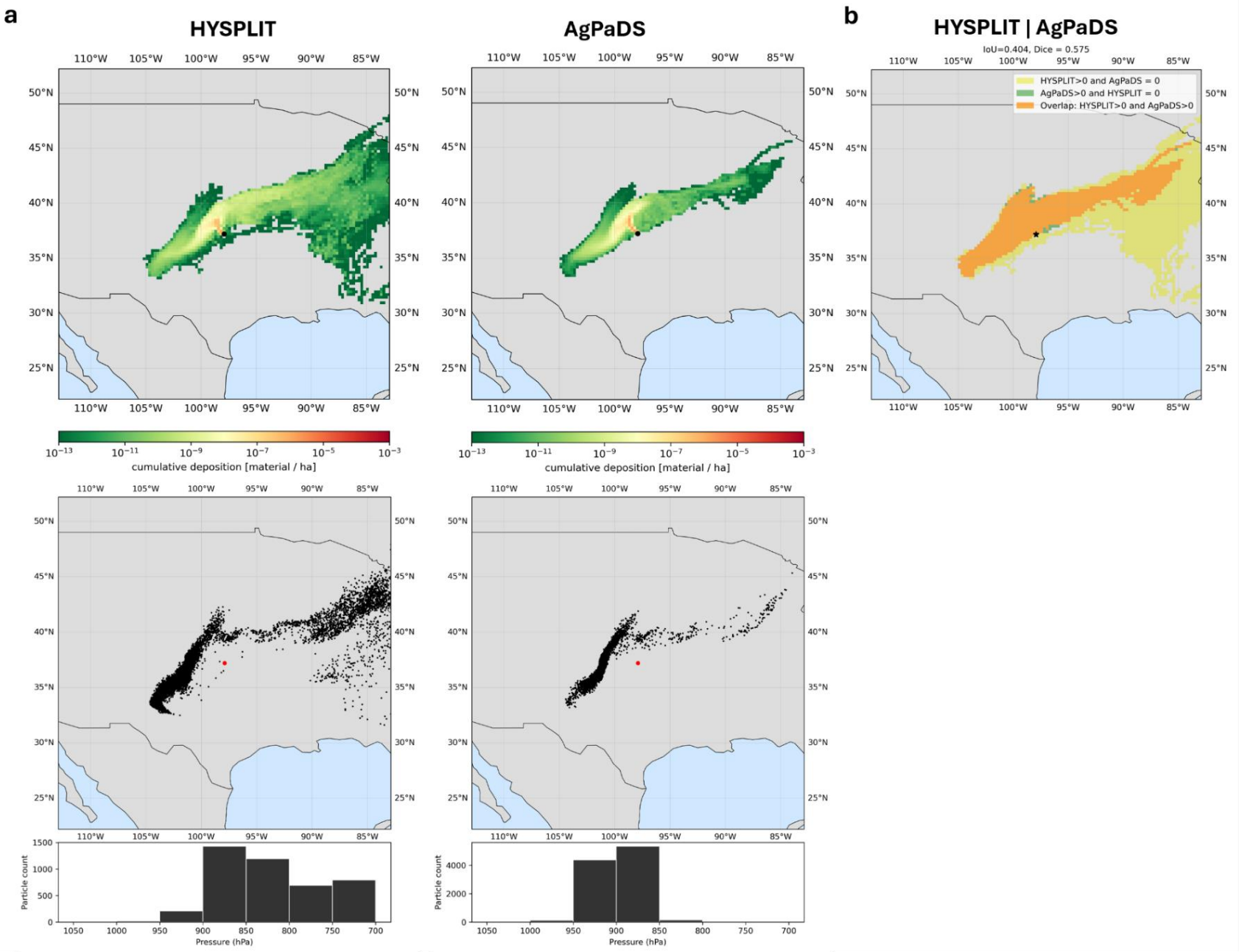

Figure S35: Comparison of time-backwards mean trajectories in HYSPLIT and AgPaDS.

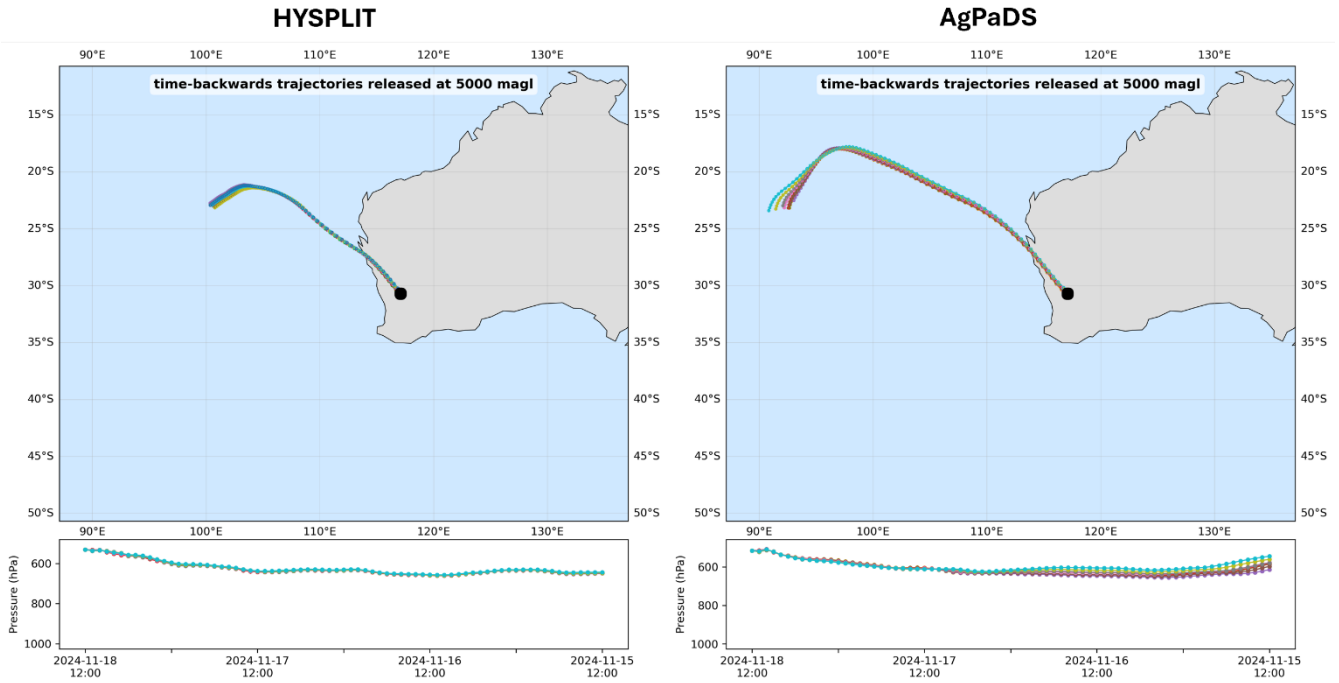

Figure S36: Performance measurements of baseline implementations

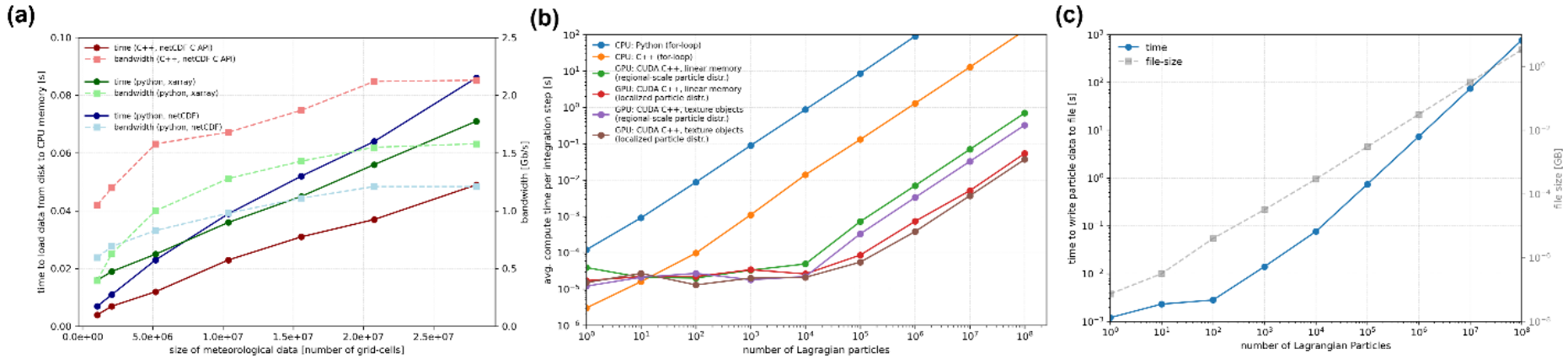

Model discussion

Table S4: AgPaDS domains of use – discussion of applicability and feasibility

domain of use	applicability & feasibility
hardware: designed on single GPU workstation and expected to scale efficiently on HPC GPU resources Example use scenarios: - researcher/modeler with one good GPU but without access to HPC resources - HPC GPU for conducting large-scale numerical experiments	• minimum hardware requirement is a CUDA capable GPU • key performance bottlenecks are disk reading speed, GPU memory size and number of CUDA cores • using high-end HPC GPUs would provide the required additional GPU memory to allow for increases in the resolution of global meteorological data and number of Lagrangian particles and it would facilitate improved performance of particle advection calculations by providing more CUDA cores for massively parallelized compute routines
wide range of **spatial scales** (from landscape to global) Example use scenarios: - global scale assessment of airborne connectivity of agricultural landscapes using ECMWFs ERA5 data - analyze European windborne crop pathogen transmission pathways of novel rust strains using regional ICON/UKMO data - national and landscape scale modelling of insect pest flight using re-gridded high-resolution ICON data for Germany	• model concept, architecture and implementation is suitable for a wide range of spatial scales • simulation model requires as input meteorological data on a regularly spaced latitude-longitude-pressure grid • conversion of different types of gridded NWP data (e.g., ERA5, ICON, UKMO UM; refs) to the required netCDF format is straightforward using tools like e.g. CDO • memory requirements: three time-steps of meteorological data need to fit into GPU memory • Lagrangian particle models have the advantage that, in principle, they can also be run using meteorological data from individual weather stations instead of gridded data, but this has not yet been implemented in AgPaDS
wide range of **temporal scales** (from climatology to forecasting) Example use scenarios: - investigate seasonal trends - examine changes in transmission risks under changing climate - short-term forecasting from latest detection sites	• simulation is implemented based on a time-streaming algorithm that requires loading of 3 time-steps of meteorological data at any time-step, so that long time extents are not a bottleneck for simulation memory or compute. The time resolution is determined by the meteorological input data. • substantial disk space is required for storing global meteorological data for long-term assessments • ECMWF releases global forecasting data for free. This data can be converted to the generic netCDF format required by AgPaDS so that the model can be used for short-term forecasting (not yet tested).
exploratory 3-D visual analyses of atmospheric transport processes Example use scenarios: - interactive definition of sources in a complex 3-D scene embedded into the AgPaDS GUI with subsequent inspection of atmospheric transport patterns, forward and backward in time, and changes of meteorological variables along the dispersing particle cloud	• the custom implementation of computer graphics routines allows for exploratory visual analysis by means of interactive 3D visualization of input data and in situ visualization of simulation data • two key bottlenecks for smooth real-time visualization are (i) memory bandwidth for loading of meteorological data from disk and (ii) number of GPU cores for massively parallelized integration of large numbers of Lagrangian particles.

thematic focus on crop diseases and insect pests
 	
Example use scenarios:
- analyze effects of meteorology on pathogen biology during atmospheric transport
	• examples of AgPaDS model components supporting applicability in crop epidemiology include
	  ○ gridded heterogeneous crop landscape source term
	  ○ selection of different pathogen viability functions

- apply AgPaDS to specific use-cases such as recent global dispersal events of wheat yellow rust - tight coupling to epidemiological models for representing realistic wind dispersal - integration into early warning systems and forecasting on global scales - develop and test new model sub-components tailored to research questions, available data and experimental setups in crop epidemiology	○ efficient simulation of extremely large numbers of Lagrangian particles • with the appropriate input data these enable e.g. ○ assessing windborne transmission risks from large numbers of disease/pest detection sites without necessity for dedicated HPC facilities ○ gridded release covering large crop growing areas (e.g., entire country, endemic region) to identify high/low risk areas or more/less likely origins of first incursion events ○ assessing the effects of landscape structure on windborne pathogen transmission risks ○ efficient calculation of airborne transport quantities required for constructing connectivity networks to improve surveillance and control.